SILVER NANO POLYMER COMPOSITE MEMBRANE
FOR HYDROGEN SULFIDE SENSING

Muhammad Bagus Arif

A Thesis Submitted in Partial Fulfilment of the Requirements
for the Degree of Master of Science
The Petroleum and Petrochemical College, Chulalongkorn University
in Academic Partnership with
The University of Michigan, The University of Oklahoma,
Case Western Reserve University
2019

Thesis Title: Silver Nano Polymer Composite Membrane for Hydrogen Sulfide Sensing

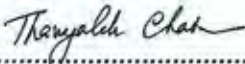**By:** Muhammad Bagus Arif

Program: Polymer Science

Thesis Advisors: Asst. Prof. Stephan Thierry Dubas

Accepted by The Petroleum and Petrochemical College, Chulalongkorn University, in partial fulfilment of the requirements for the Degree of Master of Science.

.... College Dean

(Prof. Suwabun Chirachanchai)

Thesis Committee:

....

(Asst. Prof. Stephan Thierry Dubas)

....

(Assoc. Prof. Thanyalak Chaisuwan)

....
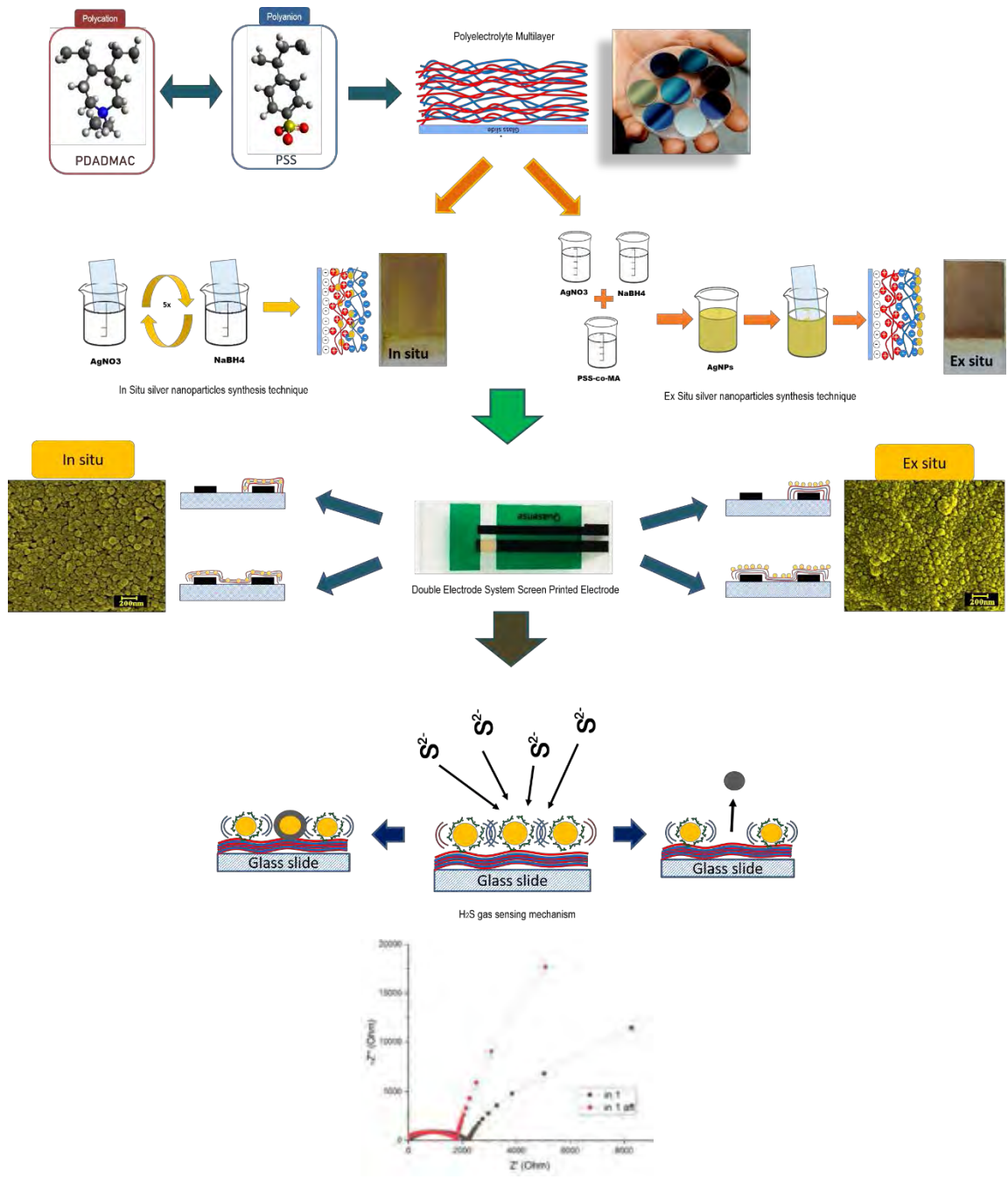
(Asst. Prof Bussarin Ksapabutr)

ABSTRACT

Optical and electrochemical sensor for H_2S sensing were developed using silver nanoparticles (AgNPs) immobilized onto polyelectrolyte membranes (PEMs) as substrate. Two approach for the deposition of the silver nanoparticles namely in-situ and ex-situ were compared for their sensing efficiency. The Poly(diallyldimethylchloride) (PDADMAC) and Poly(sodium styrenesulfonate) (PSS) were used to build PEMs via layer-by-layer assembly mechanism as polycation and polyanion respectively. In situ synthesis of silver nanoparticles was achieved by dipping the PEM coated substrate in silver nitrate ($AgNO_3$) solution followed by sodium borohydride ($NaBH_4$) as reducing agent. For ex situ technique, a monolayer of pre-synthesized silver nanoparticles was deposited as single top layer on the PEMs. The silver nanoparticles were synthesized by capping with a copolymer of styrene sulfonate and maleic acid at various concentrations. The successful synthesis of silver nanoparticles was confirmed using UV-Vis spectroscopy by monitoring the plasmon band peak at 400 nm which is characteristic of AgNPs. Screen printed electrodes were used for electrochemical sensing and were modified with the PEM following 2 different approach that were single electrode coating and double electrodes coating. The equivalent circuit was used to study the Nyquist plot of impedance results. Both types of composite membranes were exposed to hydrogen sulfide (H_2S) as analyte and compared by UV-Vis spectroscopy for optical sensing and LCR meter for impedance sensing. Ex situ synthesis technique had significant result for optical sensing, but in situ synthesis technique had better sensitivity for impedance sensing.

บทคัดย่อ

มูฮัมหมัด บากุส อารีฟ: คอมโพสิตอนุภาคนาโนเงินสำหรับการตรวจจับไฮโดรเจนซัลไฟด์ (Silver Nano Polymer Composite Membrane for Hydrogen Sulfide Sensing) อ .ที่ปรึกษา : ผศ. ดร. สเตฟาน เธียร์รี่ ดูบาส 50 หน้า

เซนเซอร์ชนิดใช้แสง (optical sensor) และอิมพีแดนซ์ (impedance) สำหรับงานเซนเซอร์สารปรอทนั้น ถูกพัฒนาขึ้นโดยการใช้เมมเบรนพอลิอิเล็กโทรไลต์ (polyelectrolyte membranes, PEMs) เป็นซับสเต รทสำหรับเคลือบอนุภาคเงินนาโน (silver nanoparticles, AgNPs) ในงานวิจัยนี้ มีวัตถุประสงค์เพื่อ ทำการศึกษาเปรียบเทียบกันระหว่างเทคนิคอิน-ซิทู (in situ) และเอ็ก-ซิทู (ex situ) เพื่อหาว่าเทคนิคใดดี ที่สุดสำหรับการเตรียมเซนเซอร์เพื่อตรวจสอบสารปรอท พอลิไดอัลลิลไดเมทิล แอมโมเนียมคลอไรด์ (poly(diallydimethylammonium chloride), PDADMAC): พอลิแคตไอออน และพอลิโซเดียมสไตรีน ซัลโฟเนต (poly(sodium styrenesulfonate), PSS): พอลิแอนไอออน จะใช้สำหรับการเตรียมเมมเบร นพอลิอิเล็กโทรไลต์ โดยเทคนิคเลเยอร์บายเลเยอร์ (layer-by-layer assembly) การสังเคราะห์อนุภาค เงินนาโนแบบอิน-ซิทู (in situ synthesis) ทำได้โดย จุ่มซับสเตรทลงในสารละลายซิลเวอร์ไนเตรต (silver nitrate, AgNO$_3$) จากนั้นจึงจุ่มลงในสารละลายโซเดียมโบโรไฮไดรด์ (sodium borohydride, NaBH$_4$) ซึ่ง จะทำหน้าที่เป็นตัวรีดิวซ์ (reducing agent) สำหรับการสังเคราะห์อนุภาคเงินนาโนโดยเทคนิคเอ็ก-ซิทู (ex situ synthesis) จะทำได้โดย เตรียมสารละลายอนุภาคเงินนาโนก่อน ซึ่งอนุภาคนาโนเงินในสารละลายนี้ จะถูกคลุมไว้ด้วยโคพอลิเมอร์ระหว่างสไตรีนซัลโฟเนต (styrene sulfonate) และมาลิอิค แอซิด (maleic acid) ที่ความเข้มข้นแตกต่างกัน จากนั้นจึงจะทำการจุ่มซับสเตรทลงไปในสารละลายดังกล่าว ยูวี-วิสิ เบิลสเปกโตรโฟโตมิเตอร์ (UV-VIS spectrophotometer) ถูกใช้เพื่อทดสอบสารละลายอนุภาคเงินนาโนที่ เตรียมได้ ซึ่งอนุภาคเงินนาโนนั้นจะมีเซอร์เฟซ พลาสมอน เรโซแนนซ์ (surface plasmon resonance) อยู่ที่ความยาวคลื่นประมาณ 400 นาโนเมตร ซึ่งเป็นคุณสมบัติเฉพาะตัวของอนุภาคเงินนาโน ในงานวิจัยนี้ ทั้งสองเทคนิคจะถูกนำมาใช้เพื่อดัดแปร และเคลือบผิวของอิเล็กโทรด: อิเล็กโทรดเดี่ยว (single electrode) และอิเล็กโทรดคู่ (double electrodes) วงจรไฟฟ้า (equivalent circuit) จะถูกนำมาใช้เพื่ออธิบาย แผนภาพไนควิสต์ (Nyquist plot) ซึ่งได้จากผลการทดสอบอิมพีแดนซ์ สำหรับการวิเคราะห์ความไว (sensitivity test) แก๊สไฮโดรเจนซัลไฟด์ (hydrogen sulfide, H$_2$S) จะถูกนำมาใช้แทนสารปรอท เพื่อให้ ง่ายต่อการเตรียมและใช้งาน ตัวอย่างที่เตรียมได้โดยทั้งสองเทคนิค จะถูกทำให้สัมผัสกับแก๊ส ไฮโดรเจนซัลไฟด์เพื่อทดสอบ การทดสอบเซนเซอร์ชนิดใช้แสง จะทดสอบโดยใช้ยูวี-วิสิเบิลสเปกโตรโฟโต มิเตอร์ และอิมพีแดนซ์จะทดสอบโดยเครื่องแอลซีอาร์ (LCR meter) ผลการทดสอบแสดงให้เห็นว่า การ สังเคราะห์แบบเทคนิคเอ็ก-ซิทู ให้ผลการทดสอบเซนเซอร์ชนิดใช้แสงดีกว่าอีกเทคนิคอย่างมีนัยยะสำคัญ อย่างไรก็ตามการวิเคราะห์ความไวโดยอิมพีแดนซ์ เทคนิคการสังเคราะห์โดนอิน-ซิทูกับให้ผลการทดสอบที่ ดีกว่า

GRAPHICAL ABSTRACT

Nyquist plot before and after exposure

ACKNOWLEDGEMENTS

TABLE OF CONTENTS

LIST OF TABLES

LIST OF FIGURES

FIGURE   **PAGE**

FIGURE   **PAGE**

CHAPTER I
INTRODUCTION

Large quantities of mercury's are released every day in the atmosphere and in the ocean. Those are emitted by natural sources (volcanoes, wildfire, and oceans), anthropogenic or human activities and re-emission of Hg from natural and anthropogenic sources. Mercury is a volatile compound that becomes the only one metal in liquid phase at room temperature. Because of its volatility, Mercury can expose the air easily and once it exposes the atmosphere, could stay for long time there to have long journey around the world (Lin, 2018). Moreover, decommissioning of offshore petroleum equipment platform in the gulf of Thailand that are contaminated with mercury a challenging issues.

Several methods have been applying for mercury removal including chemical precipitation, ion-exchange, reverse osmosis, membrane filtration, adsorption, and oxidation. Among them, ion exchange, liquid membrane, adsorption and oxidation are more famous based on selectivity, and cost-effectiveness of processing.

After removing mercury from desired environment, measurement of mercury left is a necessary to confirm safety values are reached. Residual mercury which left in small amount should be detected by very sensitive sensor. Then, competition to create sensing tool using engineered materials or available materials and mechanism become more intense. Some materials for sensor are almost the same for removing mercury from environment because of material properties and mechanism.

Amalgamation by gold still has strong utilization to collect and detect mercury from vapor and liquid phase. However, researchers try to engineer other materials instead of gold to detect mercury effectively. Simplicity, sensitiveness and briefness become the interesting points of engineered material. Besides using gold as material to detect mercury, in term of reducing the cost, researchers move to silver which also has good interaction to mercury. Silver nanoparticles can be synthesized by using salt as reducing agent and polyelectrolyte as capping agent to prevent aggregation between the particles. The deposition of silver nanoparticle on the substrate can be done by coating the substrate using PEMs through layer-by-layer

method. PEMs were made by assembling polycation and polyanion. PEMs provide charge on the substrate surface that can be used to attract ion through electrostatic interaction.

The purpose of this research is to detect mercury using silver nanoparticle on the substrate which by two different synthesis methods, ex situ and in situ. Ex situ is deposit silver nanoparticles on the substrate with prepared nanoparticles while in situ is the combination of preparation and deposition of nanoparticle in one process by utilizing PEMs as nanoreactor. The detection is based on analysing the change of collected data after being exposed by target analyte.

In the first part of this thesis the optical sensing of silver nanoparticles will be studied. Using uv vis spectrophotometer, shifting of the silver nanoparticles absorbance spectra were investigated. Sensitivity of silver nanoparticles in the solution were analyzed toward H_2S gas. Good sensitivity of silver nanoparticles in the solution brought idea to apply in the sensing device. In the next step, silver nanoparticles were deposited in the substrate through two synthesis technique, in-situ and ex-situ. Both in-situ and ex-situ were then exposed to various concentrations of H_2S gas and analyzed by uv vis spectrophotometer.

In the second part we investigated the electrochemical sensing of screen printed electrode modified with PEMs and silver nanoparticles. Screen printed electrode were used as portable device for sensing application. For this purpose, fundamental properties of the PEMs on EIS was investigated such as layer by layer assemblies, effect of salt toward PEMs and PEM coating on the electrode. Two coating mechanism, single coating or double coating, for double electrode system were investigated and collaborated with two silver nanoparticles synthesis technique, in-situ and ex-situ. Equivalent circuit, a schematic model was developed to simulate and identify the elements in the system to understand better the electrode. Both coating methodes collaborated with silver nanoparticles synthesis techniques then were used to sense H_2S gas.

CHAPTER II
LITERATURE REVIEW

2.1.   Mercury Resources

In nature, volcanic activities that triggered mercury emission were studied by Cabassi (Cabassi et al., 2017). Took place in Mt. Amiata and Solfatara Crater, the spatial distribution of air contaminants, Gaseous Elemental Mercury and H_2S, were evaluated. While mercury concentration of Aso Volcano's volcanic ash in Japan was investigated after the eruption during 2014-2016. Hg flux was calculated at 1160 ± 110 µg m^{-2} (Marumoto et al., 2017).

Next, high mercury emissions result from anthropogenic activities. Gold mining, coal combustion of power plants come as main major of the pollutant contributor. There are several main emission sectors such as stationary combustion of fossil fuel in power plants, industrial/commercial uses, agriculture, transportation, cement manufacture, production of ferrous and non-ferrous metals, production of aluminum, production of mercury metal, mercury emission from oil refining, production gold from large-scale and small-scale mining, mercury emission from chlor-alkali industry, mercury emission from product waste incineration and dental amalgams (AMAP/UNEP, 2013).

Power plant sector in Thailand released 844.5 kg in 2010 and will rocket up to 62.6% in 2030 (Pham et al., 2015). Throughout power plants use fossil fuel and coal as the fuel for the combustion, mercury will be generated. Cement sector is a promising industry in Thailand which has a big company. Co-incineration of waste and use of alternative fuels in cement kilns induce the increasing of Hg emission (AMAP/UNEP, 2013).

2.2.   Kinds of Hg

Mercury in the atmosphere is divided into 3 types: elemental mercury, inorganic mercury, particulate-phase Hg (Schroeder et al., 1998). Elemental mercury

(Hg^0) can be transported through air for long distance and this type is the most stable and dominant in the atmosphere. Inorganic mercury (Hg(II)) tends to be nearly from their source, more soluble in water, strong affinity for organic and inorganic ligands especially those with Sulphur. While particulate-mercury, Hg(p) (methylmercury), known as toxic and highly accumulate in living organisms, likely to be deposited at intermediate distance (Schroeder et al., 1998; Steffen et al., 2008). Particulate-phase-mercury becomes more intense to be studied because of toxicity to the living organisms such accumulation in the liver and rice (Poste et al., 2018; Tang et al., 2018).

2.3.   Mercury Amalgam

One of interesting mechanical properties of mercury is forming an amalgam. Many metals such as Cu, Ag, Au, and alkali metals can form amalgam with elemental mercury. Amalgam bond formation can be explained in the molecular orbital between mercury and metal. Elemental mercury has electronic configuration as $[Xe]4f^{14}5d^{10}6s^2$. Metal atom and mercury from chemical bond by combination of s or p atomic orbital of metal toward 6s mercury atomic orbital as seen in **Figure 2.1**. This interaction between mercury-metal is not strong but stronger than Hg-Hg bond. The driving force of this bond formation is orbital energy difference between mercury and metals (Gonzalez-Raymat et. al., 2017)
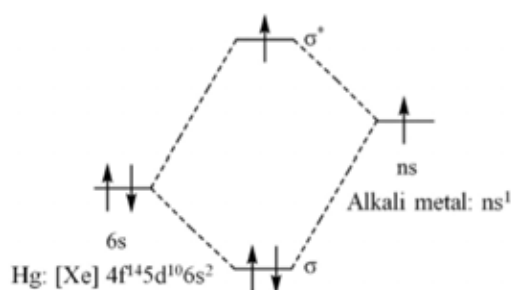
Figure 2.1. Molecular orbital diagram of Hg-metal interaction

Crystal structure and phase diagrams of alkali metal amalgam such as lithium amalgams, Sodium amalgams, Potassium amalgams, Rubidium amalgams, and Cesium amalgams had been reviewed by Deiseroth (Deiseroth, H. J., 1997).

2.4. Mercury Sensor

After removing mercury from desired environment, measurement of mercury left is needed. Then, competition to create sensing tool using engineered materials or available materials and mechanism become more intense. This section tries to provide information about either material or method of mercury sensor. Some materials for sensor are almost the same for removing mercury from environment because of material properties and mechanism.

2.4.1. Regulation of mercury standard (category of acceptable concentration)

Toxicity of mercury brings harm to environment and industrial process. Thus, US Environmental Protection Agency (US EPA) released acceptance standard of mercury concentration in the environment by criterion maximum concentration (CMC) and criterion continuous concentration (CCC) for freshwater and saltwater. CMC and CCC for freshwater are 1.694 µg/L and 0.9081 µg/L respectively and so 1.8 µg/L and 0.94 µg/L for saltwater (US EPA, 1995).

Table 2.1. Mercury concentration air and precipitation (EC, 2002)

Mercury species	In Air	In Precipitation (ng L^{-1})
Total Mercury	1.2 - 3.7 (ng m^{-3})	5 - 80
Elemental Mercury Hg(0)	1.0 - 3.6 (ng m^{-3})	< 0.005
Reactive Gaseous Mercury (RGM)	1 – 50 (pg m^{-3})	5 - 50
Total Particulate Mercury, TPM	1 – 50 (pg m^{-3})	5 - 50
Methyl Mercury, MeHg	1 – 20 (pg m^{-3})	0.005 - 0.5

For mercury contaminant in atmosphere is shown in **Table 2.1.** Methyl mercury is decided as the lowest contaminant concentration tolerated in air and to around 1-20 pg/m^3 and bellow 0.5 ng/L in precipitation because of the toxicity than other species. Reactive Gaseous Mercury and Total Particulate Mercury concentration should be under 50 pg/m^3. Where elemental mercury that dominates percentage of total mercury concentration should not be more than 3.6 ng/m^3 in air and 0.005 ng/L in precipitation because of its property.

2.4.2. Sampling Mechanism

Concentration of mercury in the environment can be known by collecting sample of fishes in an aquatic observed place or taking sample of water directly. Mercury is transported through food chain in the environment from microorganism to predator. So, bigger predator fish will contain more mercury than smaller predator fish. US EPA uses fishes to categorize level of mercury concentration such in Table 2:

Table 2.2. Fish species and mercury concentration value

Species	Estimate Chronic Value
Rainbow trout (*Onchorynchus mykiss*)	0.42 μg/L
Coho Salmon (*Onchorynchus kisutch*)	0.37 μg/L
Bluegill (*Lepomis macrochirus*)	0.25 μg/L

(US EPA, 1995)

Sample of mercury in gas feed of natural gas processing can be collected through wet collection and dry collection method where wet method uses permanganate solution and dry method use amalgamation mechanism of mercury

with gold or silver by gold coated with silica trap (Wilhelm et al., 2000, El-Feky et al., 2018)

Exposure of mercury in human can be analyzed by hair and blood with the ratio of mercury in hair-to-blood is around 250 : 1 . Therefore, hair acts as a precise hint of mercury contaminant in human body (European Communities, 2002). Besides hair, fingernail could be used to measure the mercury long-term exposure from contaminated drinking water (Wongsasuluk et al., 2018).

Table 2.3. Methods of mercury detection

Method		Reported Detection Limits
Colorimetric methods		0.01 - 0.1 µg/g
AAS	graphite furnace (GF AAS)	1 ng/g
	cold vapour (CV AAS)	0.01 - 1 ng/g
AFS	cold vapour (CV AFS)	0.001 - 0.01 ng/g
NAA	instrumental (INAA)	1-10 ng/g
	radiochemical (RNAA)	0.01 - 1 ng/g
GC	Electron Capture Detector	0.01 - 0.05 ng/g
	Atomic Emission Detector	~ 0.05 ng/g
	Mass Spectrometer	0.1 ng/g
	CV AAS/AFS	0.01- 0.05 ng/g
HPLC	UV	1 ng/ml
	CV AAS	0.5 ng/ml
	CV AFS	0.08 ng/ml
	Electrochemical detectors	0.1-1 ng/ml
ICP-MS		0.01 ng/ml
ICP-AES		2 ng/ml
Photo-acoustic spectroscopy		0.05 ng
X ray fluorescence		5 ng/g - 1 µg/g
Electrochemical methods		0.1 - 1 ng/g
Gold-film analyzer		0.05 µg/g

(EC, 2002)

2.4.3. <u>Analyzing Methods</u>

Different phase, so different method will be used to determine the concentration of mercury. **Table 2.3** shows kinds of method to analyze concentration of mercury from sample. Cold vapor atomic fluorescence spectrometry is shown to has lowest detection limit to around 0.001 – 0.01 ng/g compared to other methods. CVAFS could be used to detect mercury in solid, liquid or gas phase by treating the sample to be fit for analyzing. CVAAS and CVAFS could be collaborated with Gas Chromatography (GC) or High-Pressure Liquid Chromatography (HPLC) for several samples to get better result. X ray fluorescence could not detect the concentration bellow 5 ng/g.

2.4.4. <u>Solid phase</u>

Mercury in solid and solution can be determined by thermal decomposition collaborated with amalgamation and atomic absorption detection based on US EPA Method 7473. Where, thermal decomposition is an application of heat to degrade sample component by volatility property. So, after decomposition by heating, mercury vapor is trapped by amalgamator and then flow through absorption spectrophotometer as shown in **Figure 2.2**. The instrument detection limit for this method is 0.01 ng of total mercury (US EPA, 2007).
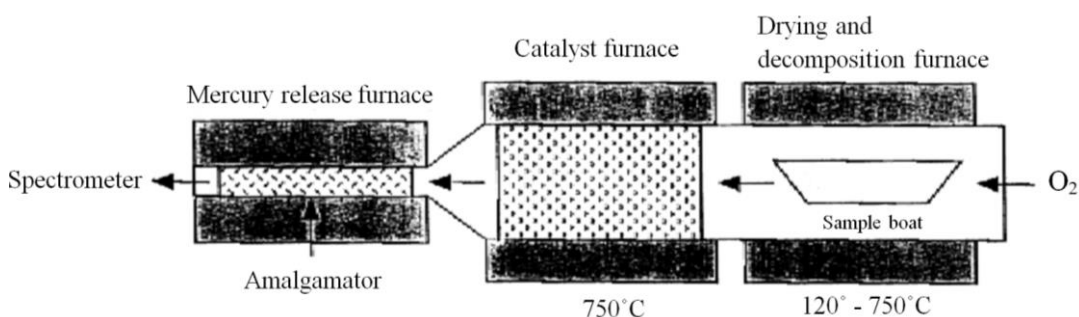
Figure 2.2. US EPA method 7473 for mercury analysis.

Solid sample of mercury in organic material such as tissue, sludge, soil and plant can be measured by CVAFS by applying digestion mechanism before analyzing.

2.4.5. Liquid phase

El-Feky et al., 2018 and Ariya et al., 2002 used Cold Vapor Atomic Absorption Spectrometry (CVAAS) based on US EPA Method 245.1 for sample analyzation. This method could be used to measure total mercury concentration in water. Water sample is digested in potassium permanganate-potassium persulfate solution and oxidized. Mercury in the digested sample will be reduced to elemental mercury by chloride and measured by cold vapor technique as shown in **Figure 2.3** (US EPA, 1994).
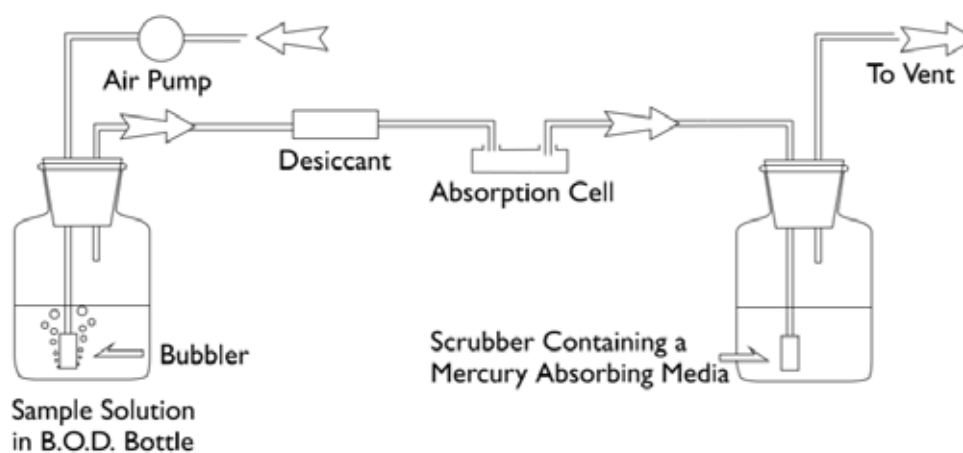
Figure 2.3. Apparatus for flameless mercury determination.

Another method for liquid phase mercury detection is ultrasonic nebulization inductively coupled plasma-atomic emission spectrometry and complex mechanism of distillation, aqueous ethylation, purge and trap, and CVAFS based on US EPA method 200.15 and 1630.

2.4.6. <u>Gas phase</u>

For determination of atmospheric mercury at vapor and particulate phase, dual amalgamation Cold Vapor Atomic Fluorescence Spectrometry (CVAFS) by gold trap based on US EPA method IO-5 is used. First amalgamation is to adsorb mercury from atmosphere in gold surface. Collected mercury is then heated and carried to analytical trap, second amalgamation and being analyzed by CVAFS. The detection limit by this method for particulate and vapor phase is 30 pg/m^3 and 45 pg/m^3 respectively (US EPA, 1999). **Figure 2.4** showed collecting sampling mechanism.
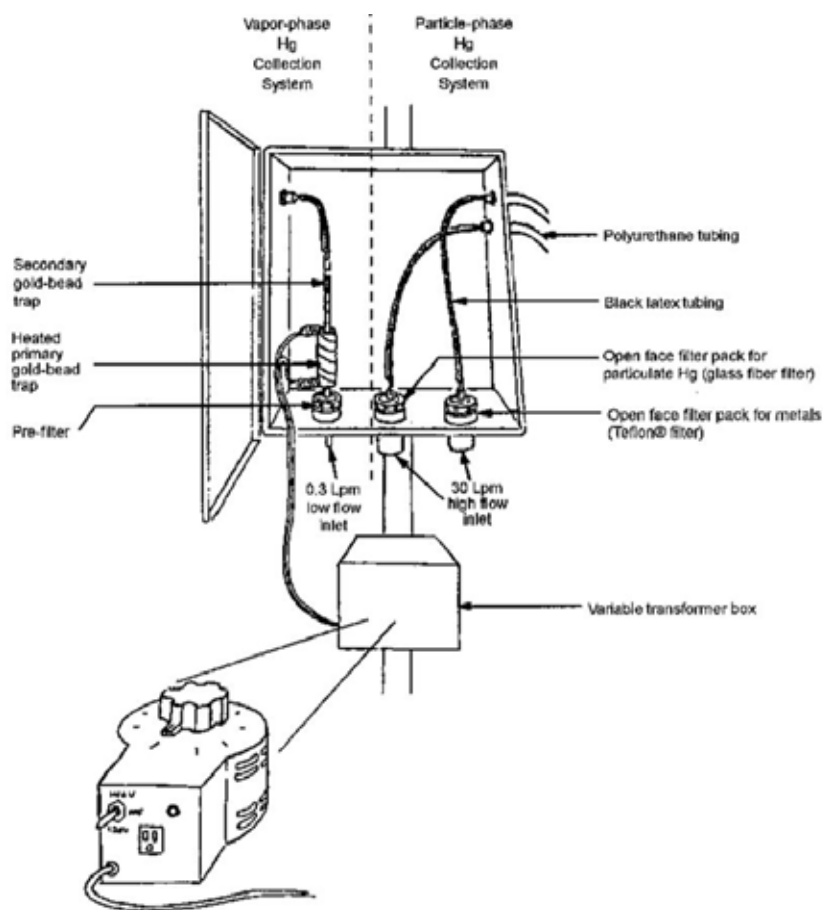
Figure 2.4. Ambient sampling system for collection of vapor and particle phase mercury (US EPA, 1999).

2.5. Hydrogen Sulfide

Another toxic gas which is in hot issue range is Hydrogen sulfide. Hydrogen sulfide is a colorless rotten egg odor gas. Hydrogen sulfide resources are natural gas, crude petroleum, hot spring, also from industrial section are petroleum or natural gas drilling and refining, wastewater treatment, cake oven, landfill and decay from bacterial breakdown (Pandey et.al., 2012).

Hydrogen sulfide bring harm to human and industry at high concentration. For human, it disturbs respiratory system through inhalation and causes death at fatal condition. At low concentration it causes unconsciousness and smell problem. Where in industrial sector, it can damage the equipment in the flow process by corrosion and decreasing the value of the final product.

In term of hazardous substance, exposure limit for hydrogen sulfide is then established. For 8-hour working time, exposure limit is 20 ppm and 10 minutes for single time exposure. For general condition in the working area, exposure limit must not more than 10 ppm (OSHA, 2019).

2.6. Colorimetric Sensor

A Simple, rapid and sensitive sensor to determine Hg species is an interesting project. People try to develop mercury sensor using gold nanoparticles and silver nanoparticles as colorimetric sensor because of the color change. The idea is because change in color can be detected by naked eye. Color change of AuNPs and AgNPs solution because aggregation of the particle in the present of mercury.

The change color of gold and silver from bulk material to nanosized particles caused by change of the resonance frequency of the particles. Color appears because of some light-waves are absorbed by the particle. At certain wavelength, particle can oscillate at resonance frequency then will absorb this kind of light-wave. The oscillation of conductive nanoparticle by incident light creates dipole moment then become recognized as Local Surface Plasmon Resonance.

LSPR of nanoparticle can shift due to some factor such size and shape, distance, and coupling of two plasmonic nanoparticles. Different shapes such as triangle, sphere, cubes, nanorods will give different graph of UV-vis spectrometer result. Larger and Longer size of particle will make red-shift resonance to the spectra due to energy need to make the nanoparticles oscillate at resonance frequency (Thomas et al., 2012). In the present of plasmonic neighbor particle, local particle will sense the plasmonic resonance and also will react by decreasing or increasing the energy. The change of plasmon energy based on near-field coupling depend on the dipole moment of the neighbor particle either oppose or same position (Thomas et al., 2018).

2.7.   Gold Nanoparticles & Gold Nanorods

Instead of finding new detection material, some researchers prefer to increase efficiency and effectiveness of gold by manipulating the surface or create a nanocomposite material. Gold nanoparticles can be synthesized through wet chemical reduction mechanism of Gold ion by sodium citrate and heating the solution for several times until the color changes to red (Grabar et al., 1995). Gold nanoparticle spectra stand at the wavelength around 500nm as shown in **Figure 2.5**. Nanocomposite consists of AuNPs, rhodamine B and hexane-dithiol successfully sensed mercury by detection limit of 0.5 ng/mL (Daware et al., 2018). Paper-based analytical device which is low cost and simple was manipulated by gold nanozyme to easily inform mercury contaminant in water based on colorimetric and effective in pH 6 (Han et al., 2017). Surface modification of gold nanoparticle and silver nanoparticle by green synthesize method using L-tyrosine as reducing and capping agent created AgNPs sensitive to Hg^{2+} and Mn^{2+}ions, while AuNPs sensitive to Hg^{2+} and Pb^{2+} ions (Annadhasan et al., 2014). And many others research about AuNPs as material detection.
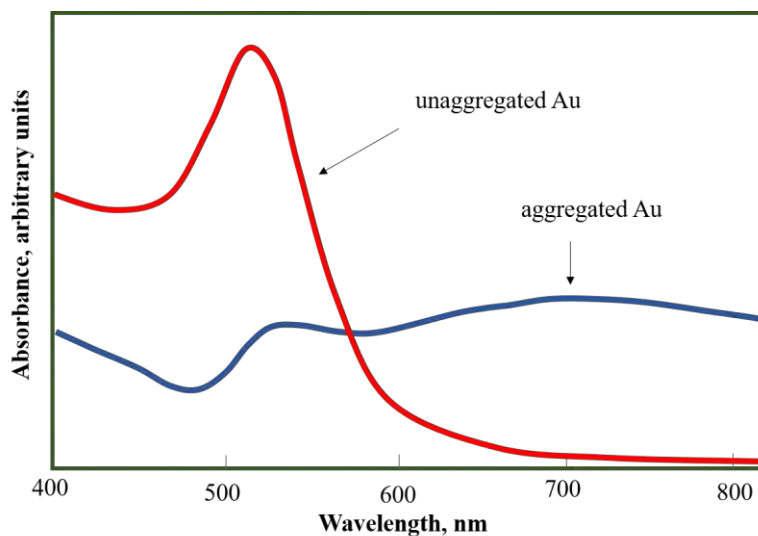
Figure 2.5. Gold nanoparticles unaggregated and aggregated absorbance spectra.

Researches want to improve the sensitivity and the detection limit, so then move to another shape which is gold nanorods. Gold nanorods has unique feature due to the dimension and change in shape after being exposure by mercury. Gold nanorods will change to be nanosphere at certain concentration of mercury. This cause by lack of shield or capping agent at the tip than the lateral side of gold nanorods, so then mercury can go through the tip and react with the gold. As the shape is changing, the color of solution also changes from blue to red (Rex et al., 2006).

2.8.   Silver Nanoparticles

In paragraph above, silver was mentioned that sensitive to Hg^{2+} and Mn^{2+}ions by green nanoparticle synthesize method. Photoelectrochemical sensor was designed by modification of TiO2 nanosheets with Au-Ag (core-shell) nanorods resulted a low detection limit around 2.5 pM (Zhang et al., 2016). Enhancing AgNPs surface sensitiveness by ligand chemistry of melamine could be used for colorimetric mercury detection by naked-eye or UV-Vis spectrometry (Kailasa et al., 2018). Recently, thiol terminated chitosan capped silver nanoparticles (Mod-Ch-Ag NPs)

was found as cost-effective mercury detection from drinking water (Sharma et al., 2018).

One method for synthesize silver nanoparticle almost the same with gold nanoparticle synthesize. The reducing agent is sodium borohydride and the stabilizer of the particle is anionic PSS-co-Maleic. No heating for this synthesizes, after mixing the solution will become yellow-orange. The stabilizer concentration controls the size of the particles, low concentration of stabilizer has larger particle than the higher one. Because of negative charge at the surface, the nanoparticle can be deposited on the substrate with opposite charge or using Polyelectrolyte Membrane (Limsavarn et al., 2006).

2.9.   Electrochemical Impedance Spectroscopy Sensor

In term of finding best method for mercury sensor and easy-used devices, trend of mercury detection moves to impedance sensor. Consider that mercury limit issued by US EPA is 10nM which less than sensing ability of conventional assay, sensitive and selective equipment is a necessary. Electrochemical impedance sensor come as a simple, low cost detection, and easy electrode modification (Hasanjani, 2019).

Impedance is a frequency-dependent measurement. The data of impedance depend on applied frequency and also phase angle. The phase angle is phase difference between voltage and current. θ is a shift caused by the response of the current or voltage to a sinusoidal potential at the same frequency of the electrode towards the applied electric stimulus as illustrate in **Figure 2.6**. To plot in the graph, θ is the angle between the directions of the real and imaginary components of Z at a given frequency, ω. For a pure capacitor, f is -90° while for a resistor it is zero (Barsoukov, E., et al., 2005)
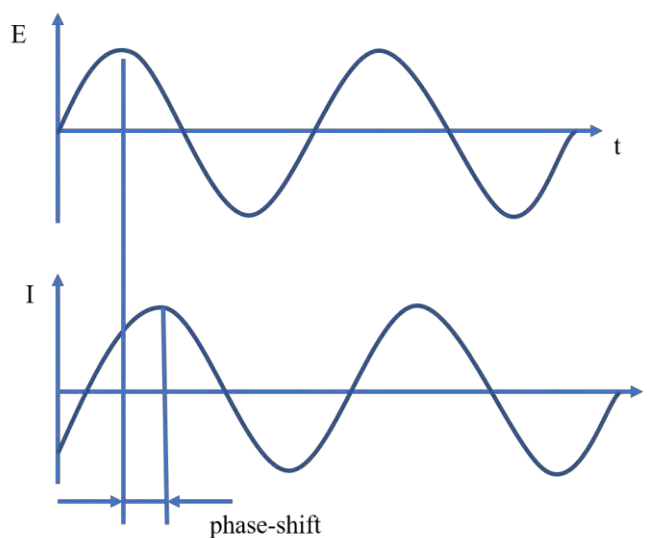
Figure 2.6. Sinusoidal Current Response in a Linear System of impedance.

The result of impedance measurement found as effect of many variables such as mass transport, rate of chemical reactions, corrosion, dielectric properties, defect, and microstructure (Barsoukov, E., et al., 2005).

Electrochemical Impedance Spectroscopy (EIS) is used to study the surface modification of the electrode. One of possible mechanism to modify the electrode surface is by using layer-by-layer assemblies. Considering the surface modification of the electrode, conductivity of the electrode will be affected then it becomes important properties to be analyzed. Simple equivalent circuit (EC) can be seen in **Figure 2.7**. From that scheme Cd represents the capacitance of the electrode surface and Rp was the polarization resistance which related to the coating resistance and other resistance in the system such as electrolyte resistance, cable resistances, and external factors were represented by Rs.
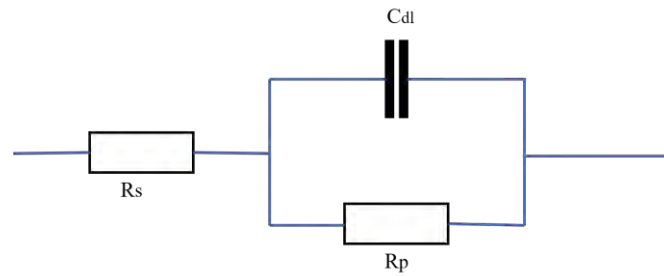
Figure 2.7. Randles cell for general simple Equivalent Circuit (EC).

Values of Rs and Rp can be determined from the frequency limit, high frequency for Rs and low frequency for Rp as shown in equation (2) and (3) respectively below:

$$Z = R_s + \frac{R_p}{1 + (j\omega C_{dl} R_p)^{\alpha}} \qquad (2.1)$$

$$Rs = \lim_{f \to \infty} |Z| \qquad (2.2)$$

$$Rp = \lim_{f \to 0} |Z| \qquad (2.3)$$

The radius of the semicircle could be known as Rp/2. Then value of Rs and Rp could be determined from the intercept of the semicircle in the real axis according to equation (1) and (2). To obtain value of capacitance Cdl could use maximum frequency of imaginary impedance Z" (fmax) vs Rp follows equation (4) below:

$$C_{dl} : \frac{1}{2\pi f_{max} R_p} \qquad (4)$$

2.10.   Layer-by-layer Assembly

First experiment had been done to manipulate the surface of a substrate using polyelectrolyte. The polyelectrolytes give electrostatic charge to the surface of the substrate. The mechanism of polyelectrolyte deposition by putting a layer onto layer of polyelectrolytes with different charge based on electrostatic interaction of macromolecules or then called by layer-by-layer self-assembly as seen in **Figure 2.8** (Decher et al., 1997).
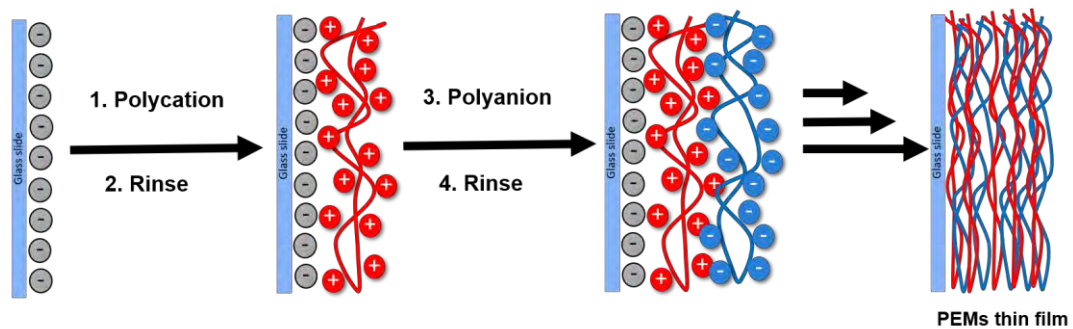
Figure 2.8. Layer-by-layer self-assembly on substrate.

In the assembling process of PEMs, polyelectrolytes are compensated through 2 mechanism, intrinsic and extrinsic compensation. Intrinsic compensation is achieved by Balancing between positive charge of polycation with negative charge of polyanion. Where, extrinsic compensation is provided by the present of supporting electrolyte. **Figure 2.9** shows charge compensation from 2 mechanism.
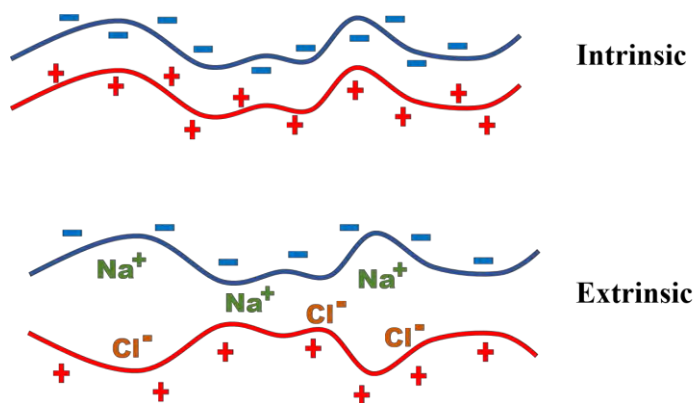
Figure 2.9. Illustration of intrinsic and extrinsic compensation

An experiment to detect mercury in the water had been done by long period fiber grating which the surface had been modified by polyelectrolyte membrane and gold nanoparticles at the outer surface. Strong polyelectrolyte membranes that consist of PSS as anion polyelectrolyte and PDAD as cation polyelectrolyte act as base and holder of the gold nanoparticle (Tan et al., 2018). Increasing number of layers will decrease the effectiveness of the surface because of the higher gap, then optimum number of layers is needed to know.

Polyelectrolyte membrane as substrate to control deposition of AgTNPs through electrostatic interaction had been done on glass slide (Detsri, 2016). AgTNPs that were synthesized by $NaBH_4$ and stabilized by citrate, has negative charge on the surface that provided by citrate. Strong polyelectrolyte PDADMAC and PSS were used for the membrane which PDADMAC as cation at the last layer. Strong polyelectrolytes were used because of their pH independent property.

CHAPTER III
EXPERIMENTAL

3.1.   Material and Equipment

3.1.1. Chemical

Sulfuric acid 96% (H_2SO_4), hydrogen peroxide (H_2O_2), ammonia 30% (NH_3), deionized water (DI), Ethanol (EtOH), poly(diallyldimethylammonium chloride) medium molecular weight 20 wt.% in water (PDADMAC), sodium chloride 99.5% purity(NaCl), poly(sodium 4-styrenesulfonaic acid-co-maleic acid) sodium salt (PSS-co-MA 3:1), sodium borohydride ($NaBH_4$), sodium sulfide anhydrous (Na_2S) and silver nitrate 99.8% ($AgNO_3$), HCl, $CuSO_4$.
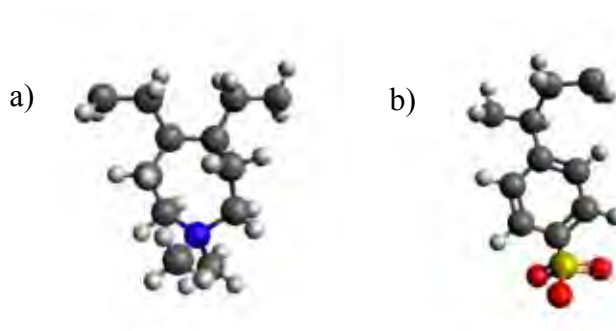
Figure 3.1. Illustration of monomer of a) PDAD and b) PSS.

3.1.2. Equipment

Double Electrode System Screen Printed Electrode (carbon and silver electrode, Quasense Co., Ltd.), Scanning electron microscope (SEM, S4800 Hitachi), UV-visible spectroscopy (Avaspec-2048, Avantes), LCR E4980A (Agilent Technologies) and AFM

3.2.   Methodology

3.2.1. Cleaning the Glass Slide / Substrate

Glass slide or substrate will be cleaned by soaking into PIRANYA and HOT AMMONIUM 20 minutes for each respectively. PIRANYA will be prepared by H_2SO_4:H_2O_2 ratio (2:1 ml) and HOT AMMONIUM will be prepared by DI water: NH_3:H_2O_2 ratio (5:1:1 ml) and solution will be heated. Finally, glass slides will be rinsed in EtOH and dried.

3.2.2. Preparation the primer on the substrate

Primer will be prepared by dipping the substrate in PDADMAC and PSS. Each of 1 mM PDADMAC and PSS will be dissolved in DI water and 1 M NaCl will be added. Glass slides will be dip in PDADMAC, DI water, PSS and DI water respectively (1 minute, 30 seconds, 1 minute and 30 seconds) for 2 layers and dipping will be finished for 5 layers and dried.

0.01 M PDAD H_2O

H_2O 0.01 M PSS
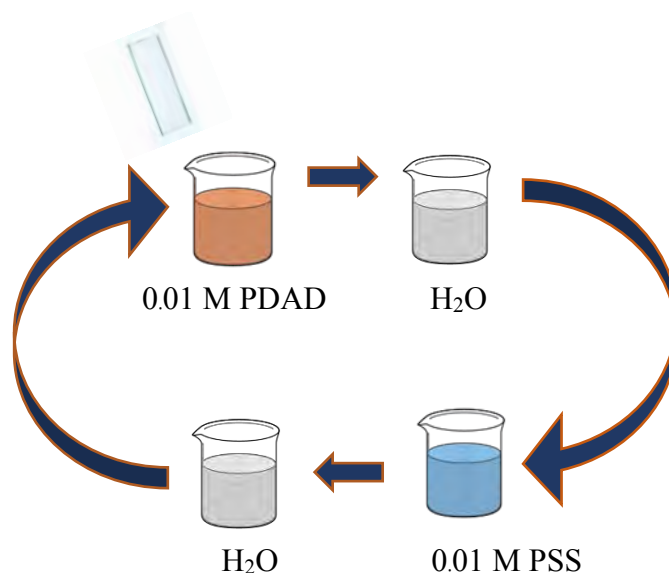
Figure 3.2. Schematic diagram of Layer-by-layer assembly mechanism

3.2.3. Preparation of AgNPs in solution

Silver nanoparticles will be synthesized through wet chemistry. $AgNO_3$ solution 1 mM and $NaBH_4$ 5 mM and various concentration of PSS-co-MA (3:1) as stabilizer will be prepared in different beakers. At first, $AgNO_3$ solution will be mixed with PSS-co-MA (3:1) at various concentration then after several minutes, $NaBH_4$ solution will be poured into the mixed solution. Leave the solution for 24 hours until the solution color changes to yellow-orange.

3.2.4. Preparation of AgNPs for coating

3.2.4.1. Ex Situ Synthesis of AgNPs

Ex situ synthesis of silver nanoparticles was done by soaking PEMs in the silver nanoparticles solution for 4 hours and rinsed. Monolayer of AgNPs was deposited on the outer layer of PEMs.
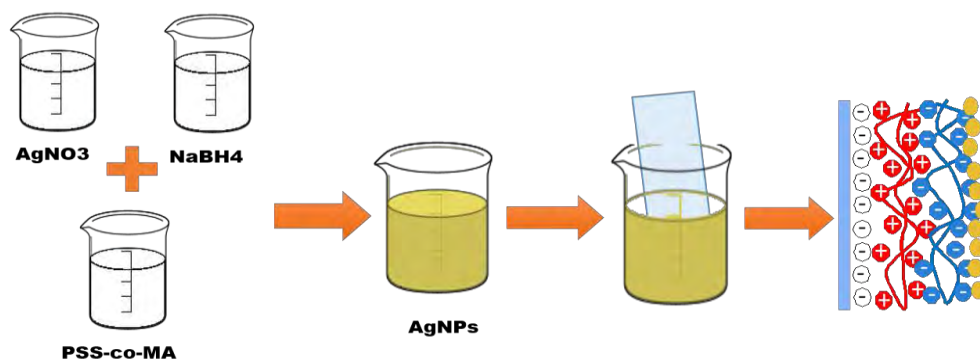
Figure 3.3. Ex-situ AgNPs synthesis technique on the substrate

3.2.4.2. In Situ Synthesis of AgNPs

In situ synthesis of silver nanoparticles was done by preparing 10mM of AgNO3 solution and 10mM of NaBH4 solution. PEMs was dipped in AgNO3 solution for 10 minutes and rinsed followed by dipping in NaBH4 and rinsed. The procedure was repeated up to 5 cycles.
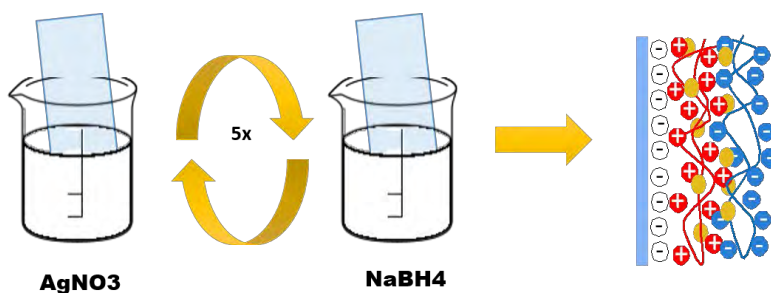
Figure 3.4. In-situ deposition of AgNPs on the substrate

    3.2.5. Testing AgNPs coated electrode sensitivity

       3.2.5.1. Optical Sensing

Two different deposition method of AgNPs was tested to detect sulfide ion by optical sensing. Deposited AgNPs on the substrate was immersed on the solution contain Na2S in various concentration (4 ppm, 0.4 ppm and 0.04 ppm). The immersion was fixed for 24 hours for each concentration to achieve maximum sulfide ion absorption by the AgNPs. Then, all substrates were dried and compared the absorbance spectra using Uv-Vis spectrophotometer.

       3.2.5.2. Electrochemical Impedance Spectroscopy Sensing

Mercury detection will be done in 2 mechanism, in water and gas. Mercury will be stored in a glass chamber and then pumped in a pipe to go to detection chamber which AgNPs coated electrode was placed inside. For liquid application, the detection chamber was filled with DI water before and bubbled with the gas flow from gas chamber. The data were measured by LCR in Z and θ mode with applied frequency between 20Hz to 2MHz which connect to user's computer. Then, excess mercury will go to gas absorber in the last chamber.
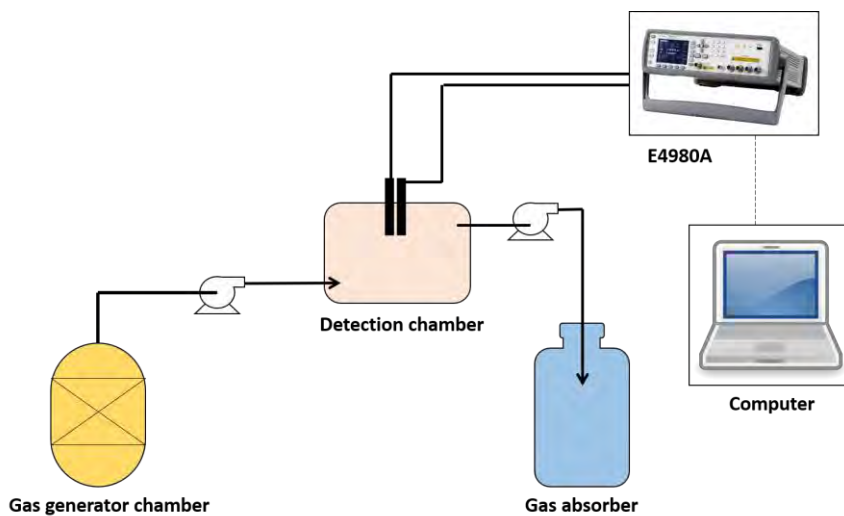
Figure 3.5. Flow process diagram of the gas detection using modified electrode

3.2.6. Preparation of H_2S gas

To make sure that N2S will react maximally, in this experiment excess HCl is used.

Na2S   + 2 HCl   → H2S   + 2 NaCl   + HCl

Feed: 1 mol/L, 100μL   1 mol/L, 1mL

  10^{-4} mol 10^{-3} mol

React: 10^{-4} mol $2\ 10^{-4}$ mol –

Product: $= 10^{-4}$ mol $+ 2\ 10^{-4}$ mol $+ 8\ 10^{-4}$ mol

MW H_2S: 34 gr/mol

H_2S weight: 10^{-4} mol x 34 gr/mol = 3,4 mg

Measurement chamber:

$$V = ¼ \times \pi \times D^2 \times H$$
$$= ¼ \times 3.14 \times 2.5^2 \text{ cm} \times 8 \text{ cm}$$
$$= 39.25 \text{ cm}^3 = 0.039 \text{ L}$$

So, H_2S in the bottle: 3.4 mg/ 0.039 L = 87 mg/L = 87 ppm (for 100% yield)

Table 3.1 Assumption of H_2S concentration from reaction

No	C_{feed} of Na_2S	H_2S (100% Yield)
1	1 M	87 ppm
2	0.1 M	8.7 ppm
3	0.01 M	870 ppb
4	0.001 M	87 ppb
5	0.0001 M	8.7 ppb
6	0.00001 M	0.87 ppb

3.3. Characterization

3.3.1. Morphology of AgNPs coating layer on electrode: SEM and AFM

3.3.2. LSPR shift: UV-visible spectrophotometer

3.3.3. Chemical testing of AgNPs and Hydrogen sulfide: Impedance LCR meter

3.3.4. Hydrogen sulfide detection: change of impedance of AgNPs coated electrode, Equivalent circuit

CHAPTER IV
RESULT AND DISCUSSION

4.1. Optical Sensing of Silver Nanoparticles in Solution

4.1.1. Effect of Capping Agent toward Silver Nanoparticles

Silver nanoparticles (Ag^0) can be achieved from silver ion through reduction mechanism by reducing agent. Silver nanoparticles are unstable and tend to aggregate to be bulk silver which have black color in solution. To prevent the aggregation of silver nanoparticles, capping agent is utilized. Capping agent will coat and prevent the aggreagation of silver nanoparticles by repulsion forces. In this experiment, different concentrations of capping agent were being studied to know the effect toward the nanoparticles and introduction for further applications.

Different concentrations of PSS-co-MA (3:1) have been used to tune AgNPs. Copolymer is chosen due to their pH-independent by sulfonate functional group. Three different concentrations, 0.05mM, 0.01mM and 0.005mM, of PSS-co-MA (3:1) were prepared during synthesis of silver nanoparticles. The copolymer solutions were mixed first with silver ions solutions, and then pour Sodium borohydride solution into the mixture. NaBH$_4$ behave as reducing agent and PSS-co-MA (3:1) acted as capping agent to stabilize the Ag^0 and prevent from aggregation by electrostatic repulsion.

Different concentrations of capping agent give different electrostatic repulsion energy due to availability number of charged molecules resulted different optical properties. In the presence of less repulsion energy, the distance between nanoparticles tend to be closer than at higher concentration and will sense neighbor nanoparticles plasmonic energy. Also, low concentration of capping agent created bigger size of nanoparticles than higher concentration and the solution has darker appearance due to the energy of surface plasmonic band. While, higher concentration provided broader particle size distribution (Limsavarn et al., 2007). Capping agent from high to low concentration coat nanoparticles as illustrated in **Figure 4.1**.
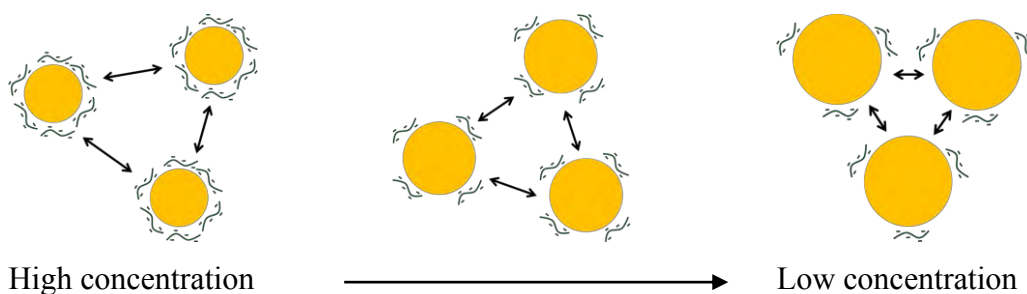
Figure 4.1. Simulation of high concentration and low concentration of silver nanoparticles capping agent.

0.005mM CoPSS-Ma has broader absorbance spectra than two other concentrations which are higher as seen in **Figure 4.2**. Broad absorbance spectra can indicate that the nanoparticles have bigger in size or close distance between each particle to sense neighbor plasmon resonance. Also, the peak shifts according to red-shift criteria, shift to higher wavelength. In condition that the nanoparticles are big, even still in nano scale, only wavelength of light which has low frequency can oscillate the nanoparticles to maximum amplitude. Low frequency is related to high wavelength and low energy.
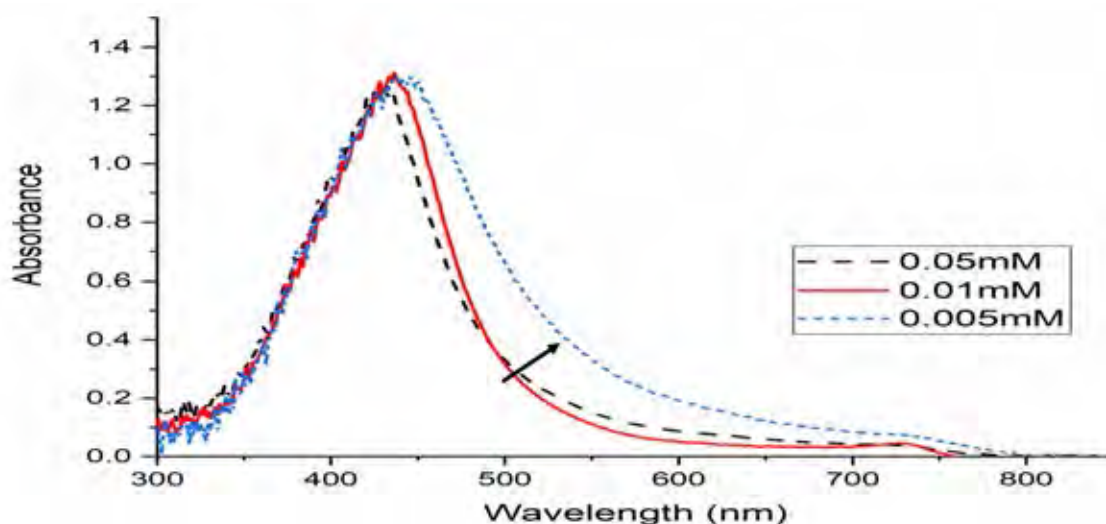
Figure 4.2. Uv-Vis absorption spectra of different capping agent concentrations and the arrows show the broadening of absorbance within decreasing concentration.

4.1.2. <u>Silver Nanoparticles on Sulfide Ion Sensing</u>

Beside preventing nanoparticles from aggregation, capping agent also modify the surface of nanoparticles by its own properties. To study this behaviour, silver nanoparticles with different concentrations of capping agent as mentioned above were tested to sense sulfide ions. S^{2-} will degrade silver nanoparticles and become Ag_2S following below reactions:

$$Ag^0 \ + \ Na_2S \qquad\qquad \rightarrow \qquad\quad Ag_2S \ + \ Na^+ \qquad (4.1)$$
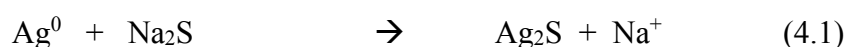
First, how fast do sulfide ions react with silver nanoparticles were analyzed. Reaction kinetics of various capping agent concentrations (0.05mM, 0.01mM and 0.005mM CoPSS-MA) were analyzed by addition 100µL of 10 mM Na_2S in 2 mL of each AgNPs solution based on SPR peak (λ_{max}) shifting as shown in **Figure 4.3. to Figure 4.5.** Within time, the peaks were experienced blue-shifting of absorbance spectra, shift to higher energy region. The shift of the peak of each absorbances were followed by a bump in the frequency about 600 nm. This region corresponds to aggregation of the nanoparticles that induced in the presence of Ag_2S as mentioned before.

0.05mM showed satisfying result by loss of absorbance peak 20% in first 10 minutes compared to 0.01mM and 0.005mM which only 10% and 4% respectively as seen in **Figure 4.6**. After 24 hours, final solution had yellow clear appearance because of surface energy loss by sulfidation (Fletcher et al., 2019). Sulfidation in the silver nanoparticles will occur at the outer surface of nanoparticles and grow inside. This sulfidation will indunce aggregation between neighbor silver nanoparticles (Schlich, K. et al., 2018).
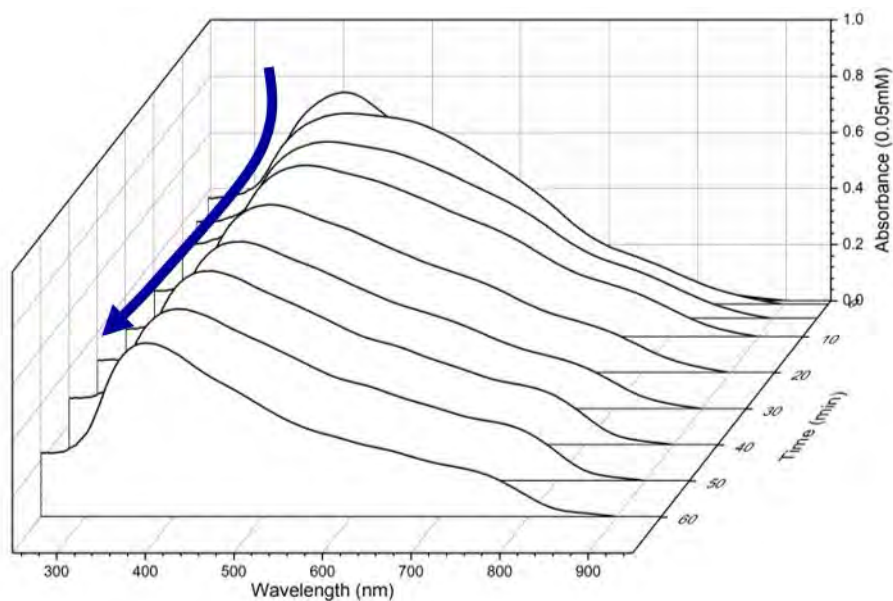
Figure 4.3. UV-Vis absorbance spectra of AgNPs synthesized with 0.05mM CoPSS-MA towards Na$_2$S 40 ppm within one hour.
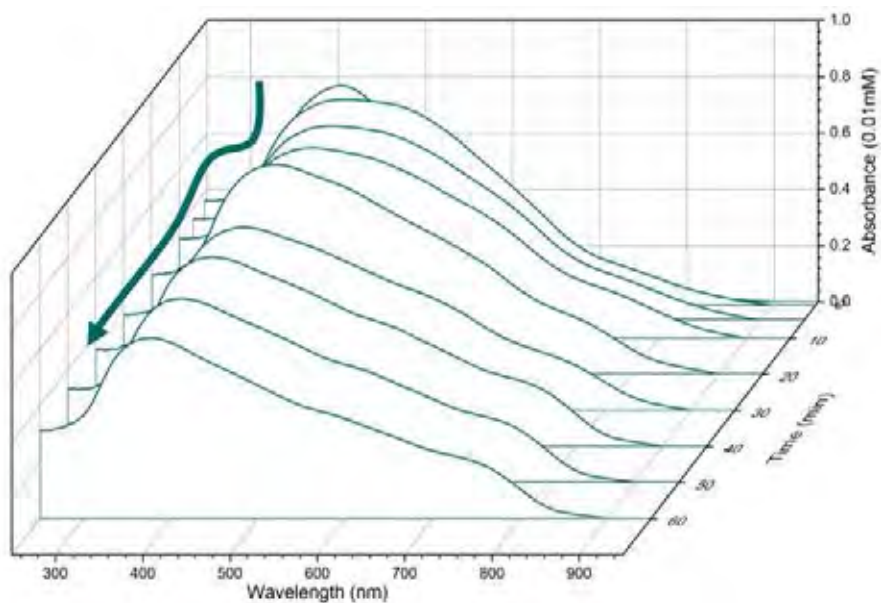
Figure 4.4. UV-Vis absorbance spectra of AgNPs synthesized with 0.01mM CoPSS-MA towards Na$_2$S 40 ppm within one hour.
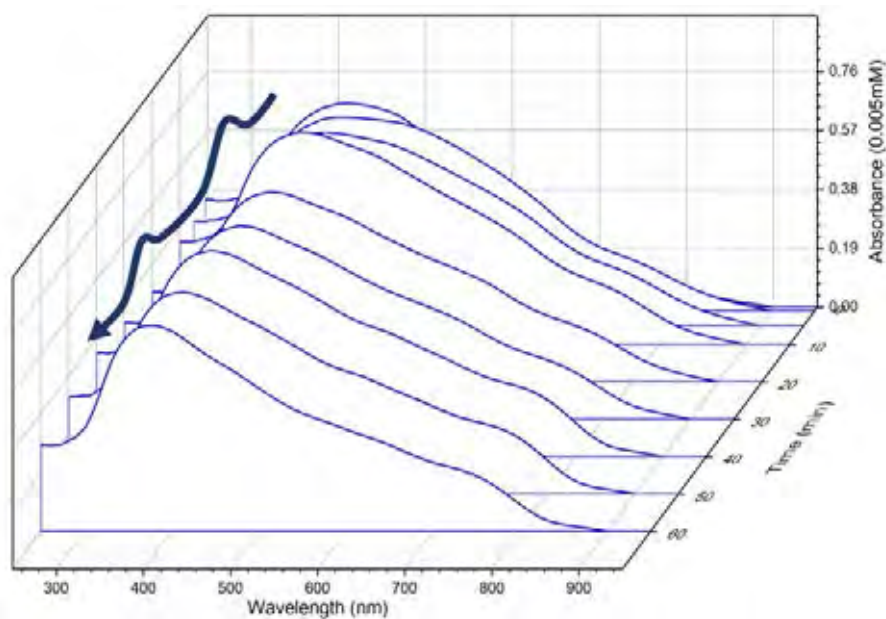
Figure 4.5. UV-Vis absorbance spectra of AgNPs synthesized with 0.005mM CoPSS-MA towards Na₂S 40 ppm within one hour.
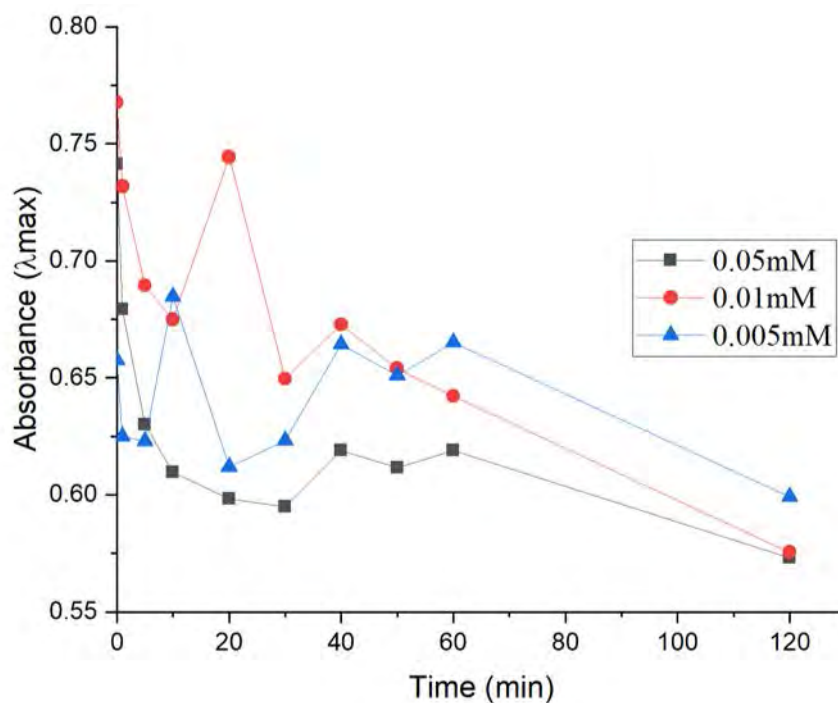
Figure 4.6. Plot of Uv-Vis absorbance peak (λ_{max}) change of each capping agent concentrations (0.05mM, 0.01mM and 0.005mM) within time toward Na₂S 40 ppm.

Several processes could cause a loss in UV-Vis absorbance such as: i) aggregation of AgNPs by Na^+, ii) AgNPs dissolution, iii) reprecipitation as Ag_2S or iv) direct AgNPs sulfidation by high concentration of sulfide ion (Baalousha et al. 2015). In the next step 0.05mM capping agent was assumed had satisfying result among two others, that concentration was used to test toward concentration of Na_2S. 100μL drop of various concentrations from 0.04 ppm to 40 ppm of Na_2S was added to 2 mL 0.05mM PSS-co-MA-AgNPs solution and check the absorbance spectra after 24 hours. In the presence of sulfide at low concentration, slightly change and almost no significant color change could be seen for addition 0.04 ppm and 0.4 ppm of Na_2S in AgNPs solution compared to 40 ppm which had significant change either in absorbance peak or solution color as shown in **Figure 4.7 A and B**.

Surprisingly, addition 4 ppm of Na_2S experienced red shifting of the plasmon band and absorbance spectra broadening. This concentration level might cause sulfide ions penetrate to AgNPs and generate aggregation but still in nanosized particles and decrease surface energy to shift the SPR peak proven by change in color (Thomas et.al., 2018).
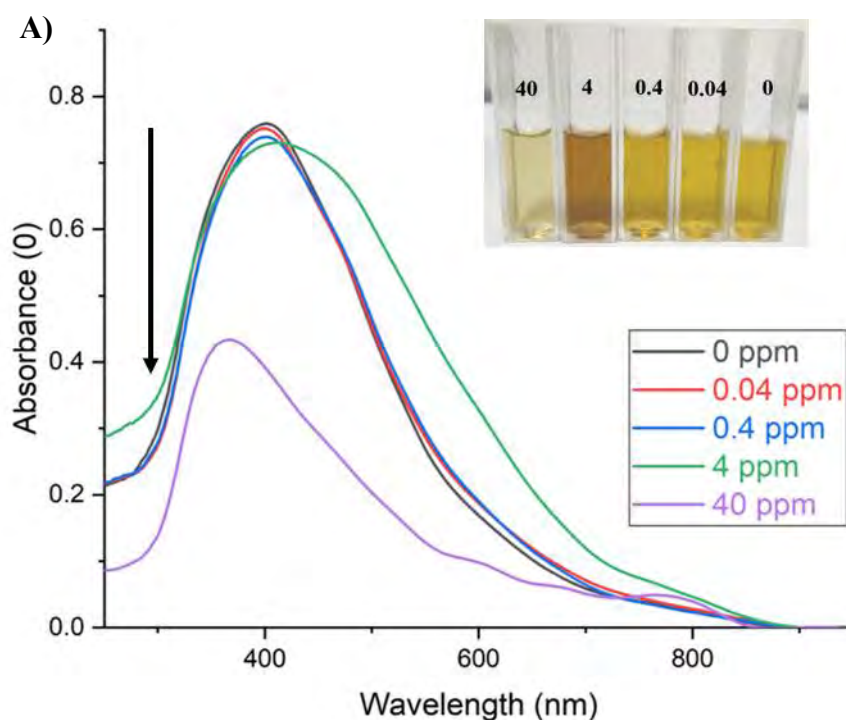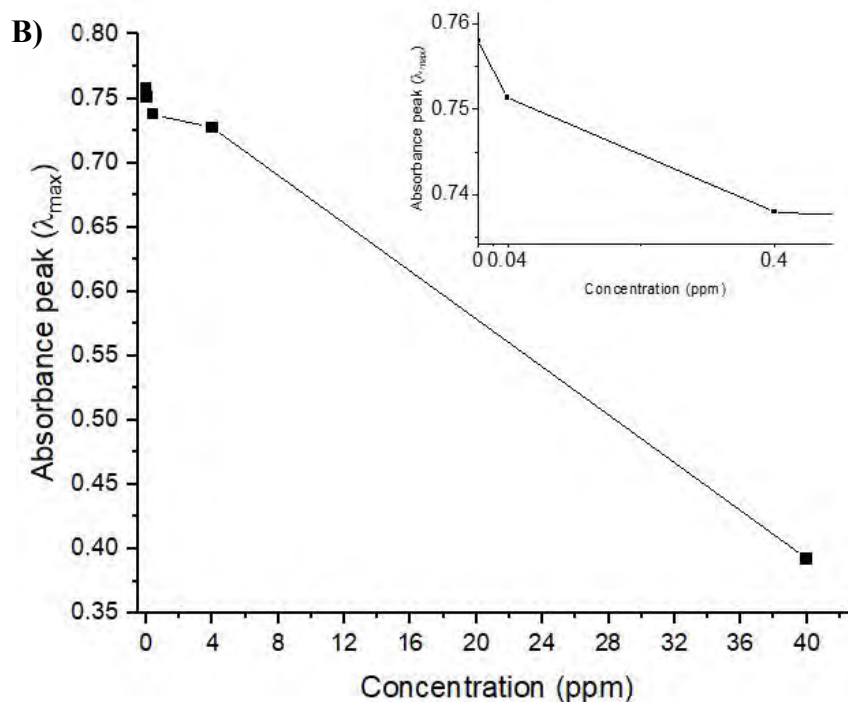
Figure 4.7. A) UV-Vis absorbance spectra of AgNPs with 0.05mM PSS-co-MA as stabilizer toward various concentrations of Na$_2$S and B) plot of absorbance peak (λ_{max}) for each spectrum. Inset: 40 ppm to 0 ppm Na$_2$S from left to right.

In other hand, various concentration of capping agent from 0.005mM, 0,01mM and 0,05mM were exposed to various concentrations of Na$_2$S in purpose of mapping and detect by Uv-Vis spectrometer. Na$_2$S concentrations were set as final concentration from 100 ppm to 1 ppb in the solution. All sulfide concentration made change to the absorbance spectra even just a slightly shift. (See Appendix A)

4.1.3. Silver Nanoparticles Synthesis Technique

To utilize silver nanoparticles on further applications, in this part is sensing application, silver nanoparticles need to be deposited on a substrate. Deposition of silver nanoparticles on substrate can be done through two synthesis mechanism, ex situ synthesis technique and in situ synthesis technique. For this purpose, Polyelectrolyte membranes which are assembled through electrostatic interation used as substrate to deposit silver nanoparticles.

Ex situ synthesis technique will deposit silver nanoparticles on the outer layer of the membranes where in situ synthesis technique will deposite silver nanoparticles inside the membranes. PDADMAC and PSS are assembled through electrostatic interaction of oppositely charged of each molecule to built PEMs. Addition of NaCl for each solution breaks ion pairing between polycation and polyanion and enhanced the mobility of molecule (Fares & Schlenoff, 2017).

4.1.3.1. Ex situ silver nanoparticles synthesis technique

First synthesis technique is ex situ synthesis technique. This technique creates monolayer of silver nanoparticles on the outer layer of the membranes. Silver nanoparticles have to be prepared before and then soak PEMs modified substrate surface in the AgNPs solution. By electrostatic interaction between capping agent and PEMs outer layer, deposition of AgNPs can be achieved.

Creating monolayer of AgNPs in the outer layer of PEMs through ex situ technique was affected by the concentration of nanoparticles stabilizer. This is because the capping agent controls the adsorption of nanoparticles. Based on experiment in the solution, silver nanoparticles with 0.05mM capping agent was chosen for this technique for its property also stable in acidic and basic solution (Limsavarn et al., 2007).

Dipping time was limited from 3 to 4 hours for maintaining the optical properties. AgNPs with well protection repel and adsorb in a less packed density to retain in yellow color (Dubas et al., 2011). AgNPs in solution have free motion because availability of space between particles so then the surface energy can stand by its own. However, for ex situ technique where AgNPs were packed together, one particle sensed neighbor energy that could decrease the surface energy. This case was proven by lower absorbance peak than in the solution and broadens, also the color appeared orange as shown in **Figure 4.8 and Figure 4.9.**
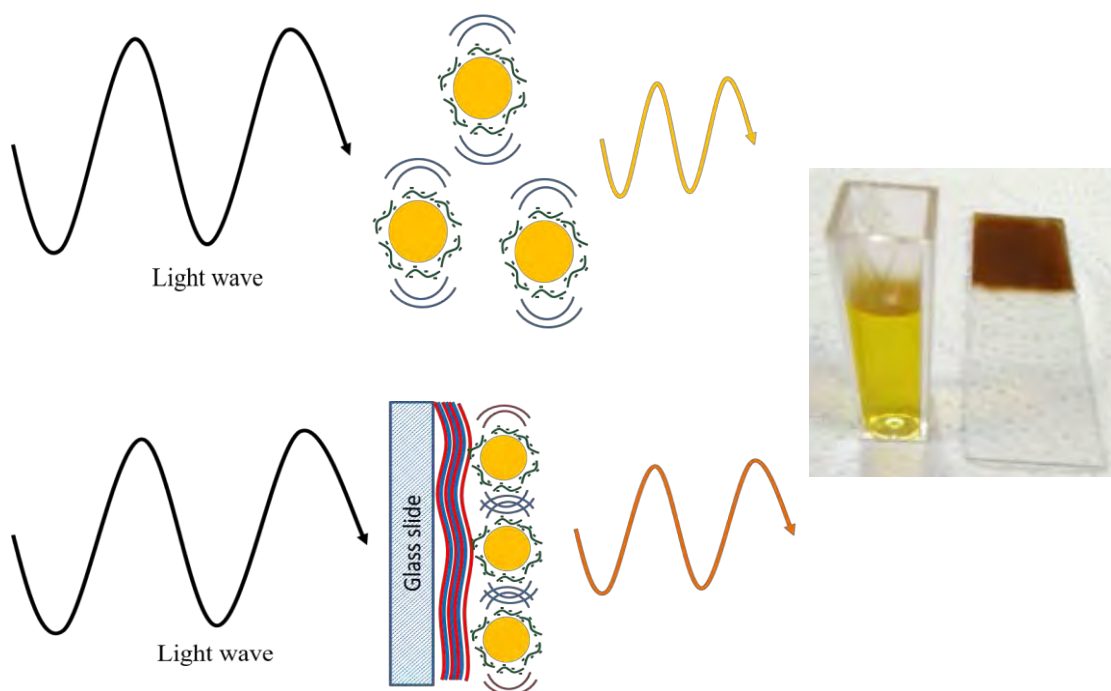
Figure 4.8. Illustration of appearing color of AgNPs with capping agent concentration 0.05mM in solution, where the nanoparticles have more space and on PEMs, where the nanoparticles have close packing and sense neighbor plasmon resonance. Inset: picture of different appearance colors from AgNPs in solution and on PEMs.
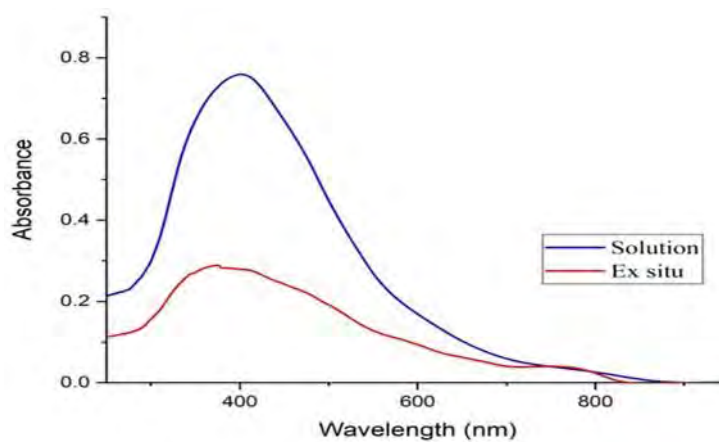
Figure 4.9. UV-Vis Absorbance spectra of AgNPs in solution and on PEMs through ex situ synthesis technique with 0.05mM of capping agent.

4.1.3.2. In situ silver nanoparticles synthesis technique

    Instead of creating silver nanoparticles monolayer on the outer layer of substrate, deposit silver nanoparticles inside the membranes is another interesting method to study. Silver nanoparticles behave as filler for composite as seen in **Figure 4.10**. This technique is then called by in situ silver nanoparticles synthesis technique (Wang et.al., 2002). Different with ex situ synthesis, silver nanoparticles are reduced from silver ion within the membranes by this technique. PEMs as substrate will be dipped in $AgNO_3$ solution for several minutes and then dipped in $NaBH_4$ solution and repeat several cycles.
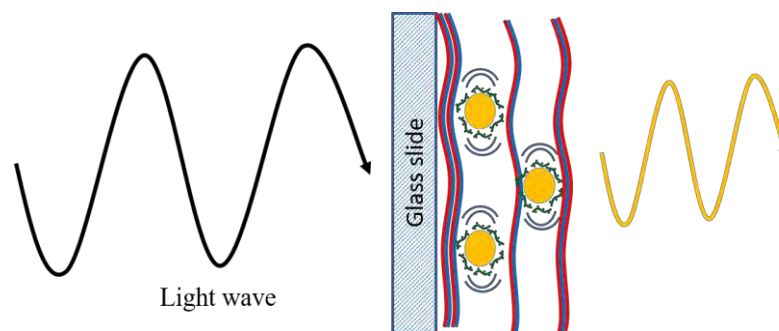
Figure 4.10. Illustration of silver nanoparticles deposition through in situ technique

    For in situ synthesis technique, AgNPs are dispersed inside the PEMs. Penetration mobility is enhanced in the presence of NaCl during PEMs assembly. Ag^+ from silver nitrate is attracted by electrostatic interaction from negatively charged molecule in PEMs. Well dispersed Ag^+ then turn to Ag^0 by reduction mechanism using sodium borohydride. When the absorbance was measured by UV-Vis spectrophotometer, AgNPs through in situ synthesis technique have higher absorbance spectra than synthesis through ex situ technique as seen in **Figure 4.11**. This might be caused by dispersion of silver nano particles inside of the membranes and the distance between each silver nanoparticles far enough from neighbor plasmon disturbance.
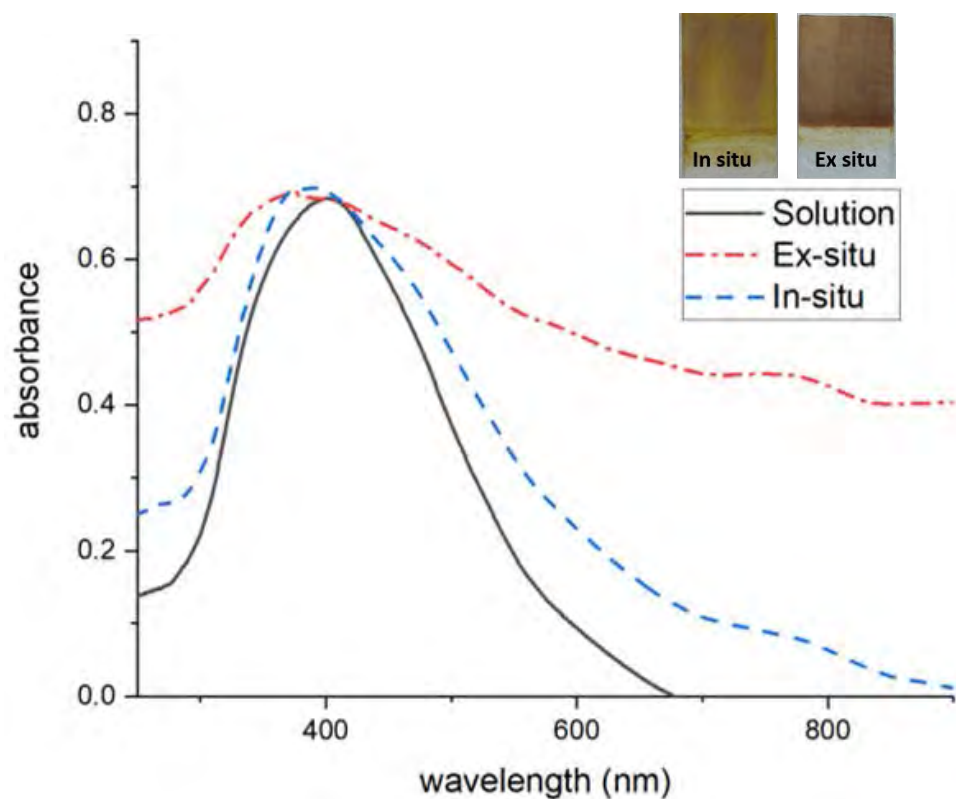
Figure 4.11. Normalized UV-Vis Absorbance spectra of AgNPs through ex situ synthesis technique from AgNPs with 0.05mM of capping agent concentration and in situ synthesis technique. Inset: AgNPs from different synthesis techniques on glass slide.

4.1.4. <u>Sulfide Ion Sensing</u>

Ex situ and in situ silver nanoparticles synthesis technique deposit silver in the composite differently. For sensing application, these mechanisms may give different result or sensitivity. Then, sodium sulfide was used as analyte to test both synthesis techniques and detected the absorbance spectras change by Uv-Vis spectrofotometer.

The prepared silver nanoparticles in different synthesis technique were then used to sense sulfide in various concentration (0.04ppm, 0.4ppm and 4ppm). It was assumed that AgNPs in the films had better sensitivity than AgNPs in the solution due to number of particles or size of the particles. Proposed schematic for sulfide ion absorption on different AgNPs deposition were shown in **Figure 4.12**.
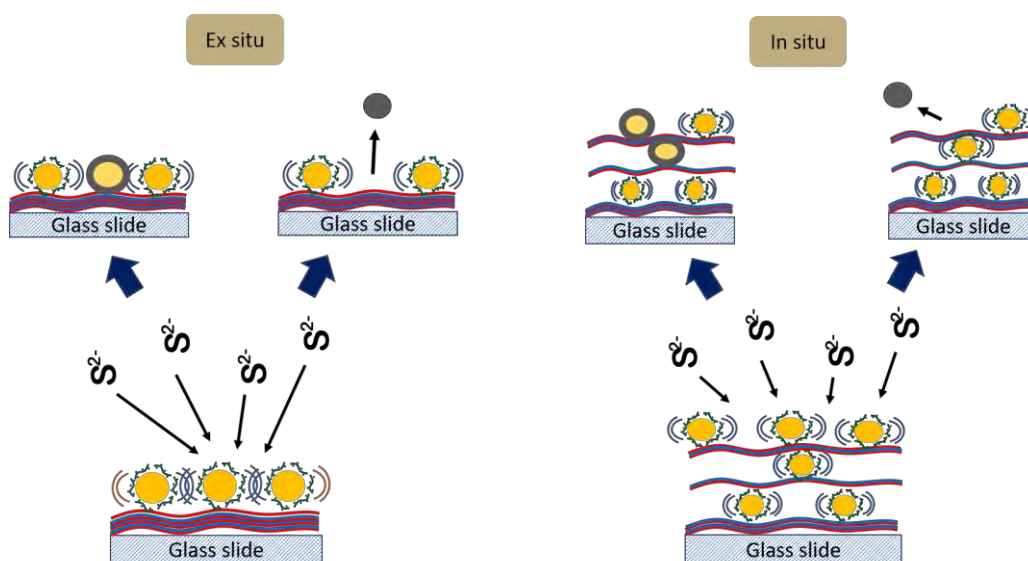
Figure 4.12. Proposed schematic of Sulfide ion absorption toward AgNPs coated substrate in different deposition technique.

It seems like for in situ deposition, S$^-$ should go through PEMs barrier to be absorbed by AgNPs inside, while monolayer of AgNPs by ex situ deposition will face S$^-$ easily. This proposed absorption mechanisms were proven by absorbance spectra results. A well dispersed AgNPs from in situ technique were experiencing a shift of surface plasmon band for all various concentrations. Where in other hand, ex situ technique showed increasing absorbance spectra after being exposed to Na$_2$S as seen in **Figure 4.13**.

Monolayers of silver nanoparticles in the films were degraded by sulfidation, then absorbance spectra might be resulted from remaining silver nanoparticles in the films. At low concentration of sulfide ion, well packed silver nanoparticles monolayer degraded a few numbers than the higher concentration. This sulfidation also let off nanoparticles from neighbor plasmon energy disturbance proven by change in absorbance spectra and optical color that can be seen by naked eye. If compared side by side, clearly seen that after exposed to 4 ppm the film showed orange color and 0.04 ppm appeared more yellow.

To clearly see a different mechanism in the shifting of absorbance spectra between ex situ and in situ AgNPs synthesis on the substrate, several

concentrations of Na$_2$S from 100 ppm to 1 ppb were used (see Appendix B). In those various concentrations of sulfide, absorbance spectra of ex situ deposition technique tend to increase in the exposure of higher concentration but vice versa for in situ deposition technique where tend to decrease.

g.
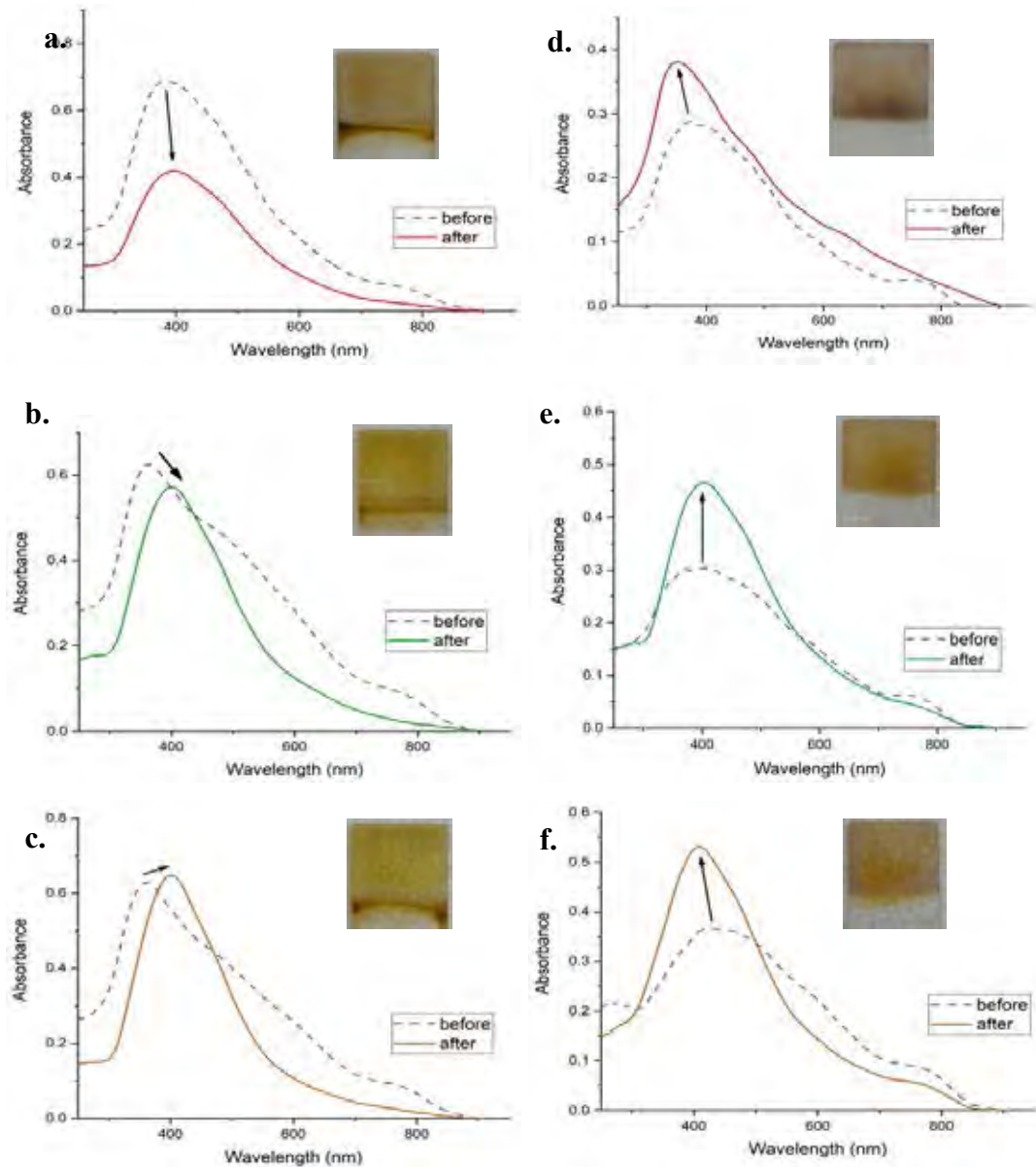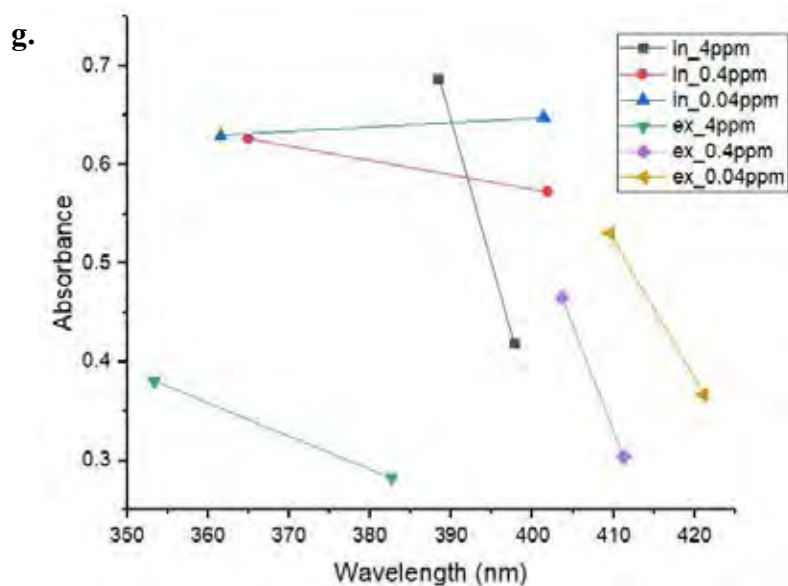
Figure 4.13. AgNPs UV-Vis absorbance spectra through in situ (a, b & c) vs ex situ (d, e & f) synthesis technique in different concentration of Na_2S: (a, d) 4 ppm, (b, e) 0.4 ppm & (c, f) 0.04 ppm. Inset: Appearance of the AgNPs on glass slide after exposure. And (g) summary of the shifting plot from the absorbance peak of each spectra.

4.2. Electrochemical Impedance Spectroscopy Sensing

4.2.1. Polyelectrolyte Membranes (PEMs) on Double Electrode System Screen Printed Electrode (SPE)

Impedance is a frequency-dependent measurement. In this experiment, modifying the electrode by build PEMs in between 2 electrodes become a matter of interest. Double electrode system screen printed electrode from Quasense Co., Ltd (Bangkok, Thailand) was used as subject electrode.

To build PEMs on this kind of electrode is very tricky. Firstly, PEMs were built using immersion mechanism, which immerse the SPE in the PDAD followed by rinsing with DI water and PSS followed by rinsing in DI water repeatedly until desired number of layers. Consider that desired current path only between the electrodes, the mechanism of PEMs assemblies changed to drop by drop as shown in **Figure 4.14**. PEMs were achieved by drop 50 μL of PDAD in between

electrodes followed by rinsing with flow of DI water and dried with air pump, then did the same mechanism with PSS, and repeat until desired number of layers. Moreover, EIS results for those both mechanisms had no difference after plotting at Nyquist plot which means the dipping mechanism can be substituted by dropping mechanism.
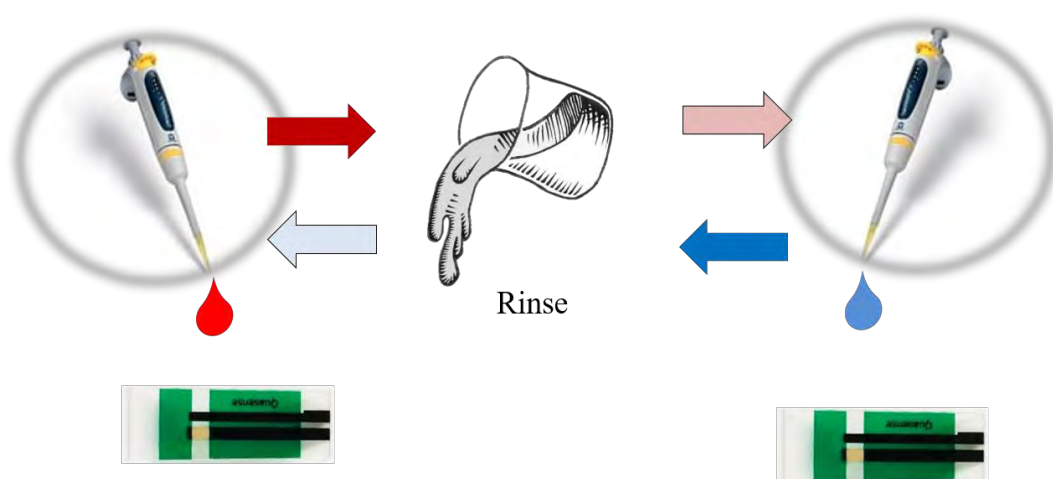
Figure 4.14. Layer-by-layer assembly through dropping mechanism.

In term of analyzing the effect of PEMs toward the electrode impedance, PEMs will be built on both electrodes and only on 1 electrode and discussed in section 4.2.3. Consider that electrostatic behaviour is different, PEMs on both electrodes assumed will act as a bridge for electron/current to go, and PEMs on 1 electrode will act as barrier for electron/current.

4.2.2. Effect of Salt concentration on PEMs assembling

During assembling PEMs, salt becomes interesting and important material. Salt can be used to tune PEMs as desired final result. In this part, smoothing and swelling of PEMs caused by salt were studied. This study will help to analyze effective salt concentration for preparing PEMs as substrate for further applications.

First, salt acts as annealing agent by immersing PEMs in the salt solution. Salt draw out water molecules of the ion pairs in PEM through osmotic pressure. This behaviour caused a smoothing of the PEMs surface Smoothing of surface was achieved in higher salt concentration (Dubas, S. T., 2001). Intrinsic and extrinsic charge compensated, intrinsic by Pol+ and Pol- interaction. Extrinsic by counter ion from supporting electrolyte as seen in reaction (4.1);

$$Pol^+A^-_{aq} + Pol^-C^+_{aq} \leftrightarrow Pol^+Pol^-_s + A^-_{aq} + C^+_{aq} \qquad (4.1)$$
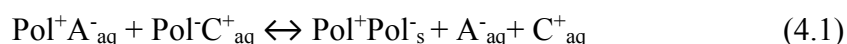
That is a reversible equation, which in the present of enough salt the reaction goes reverse and the PEM dissociate. Concentration of salt affect Pol+ and Pol- sorption into the membrane. Higher salt concentration will increase the diffusion rate (Fares, H. M., 2017).

Second, salt as supporting electrolyte. Because of charge-charge repulsion of monomer unit, polyelectrolyte behave a 'flat' conformation. In the presence of supporting electrolyte, salt ion will screen the charge-charge repulsion force between monomer unit caused polyelectrolyte to behave a 'loopy' conformation as shown in **Figure 4.15** (Decher and Schmitt, 1992). This loopy conformation related to the roughness of the PEMs final surface (Lvov, Y., et al., 1993).
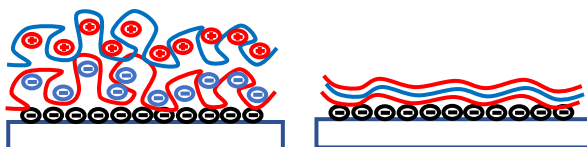
Figure 4.15. Illustration of **'**Loopy' conformation and 'flat' conformation of PEMs.

In term of impedance, PEM also being investigated under different environment such different kind of supporting electrolyte and temperature. The result was the impedance is decreasing under salt that has higher ionic strength and higher temperature (Silva et al., 2005).

For effect of salt as supporting electrolyte, in this experiment PEMs were built up under different salt concentration (0M, 0.5M, 1M and 2M) for each polyelectrolytes and measure under neutral environment (H_2O). Fixed frequency 1 kHz was applied to collect the impedance data. Generally, measurement in water show decreasing in impedance within increasing number of layers as shown in **Figure 4.16** for Nyquist plot and **Figure 4.17** at fix frequency. To be comparable, data were collected in every addition of odd number of layers for each salt concentration. Some factors that affect the impedance result is different charge of the outer layer of PEMs which depend on the polyelectrolyte type. From external disturbance factors, delamination caused by rinsing and drying process contribute to an error in the collecting data.
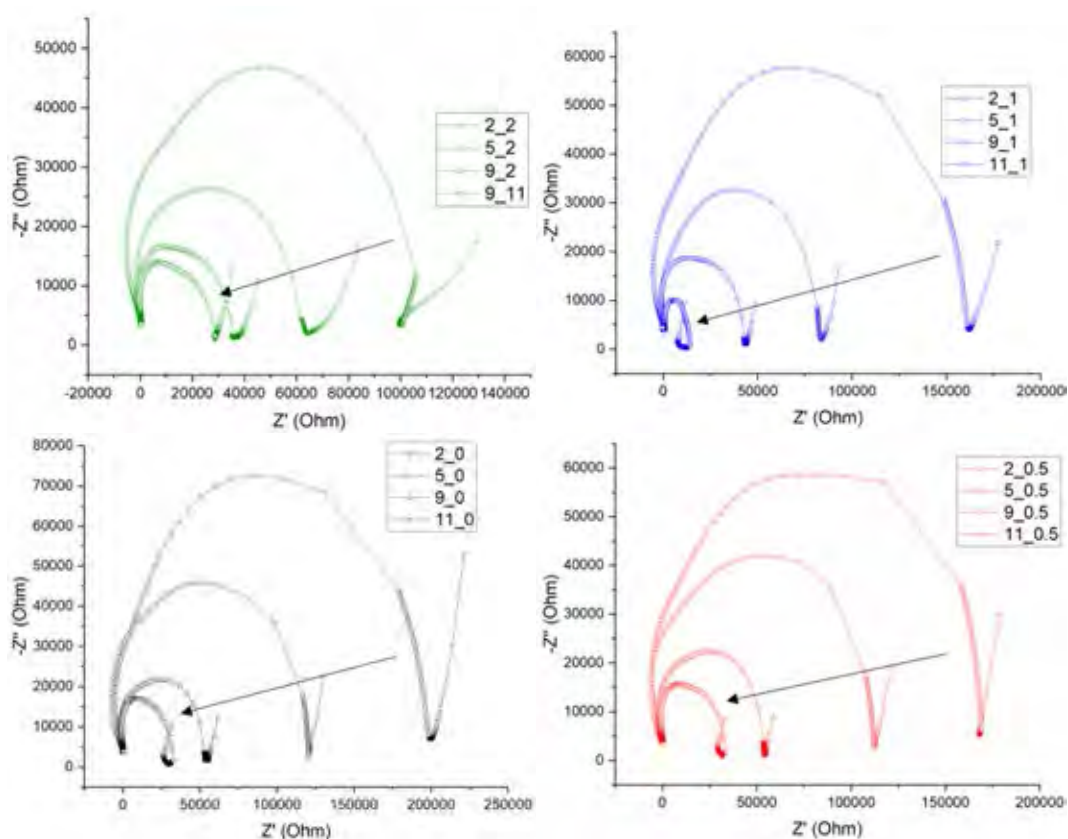
Figure 4.16. Nyquist plot of PEMs with various concentrations of supporting electrolyte (0M, 0.5M, 1M and 2M) measured in H_2O.
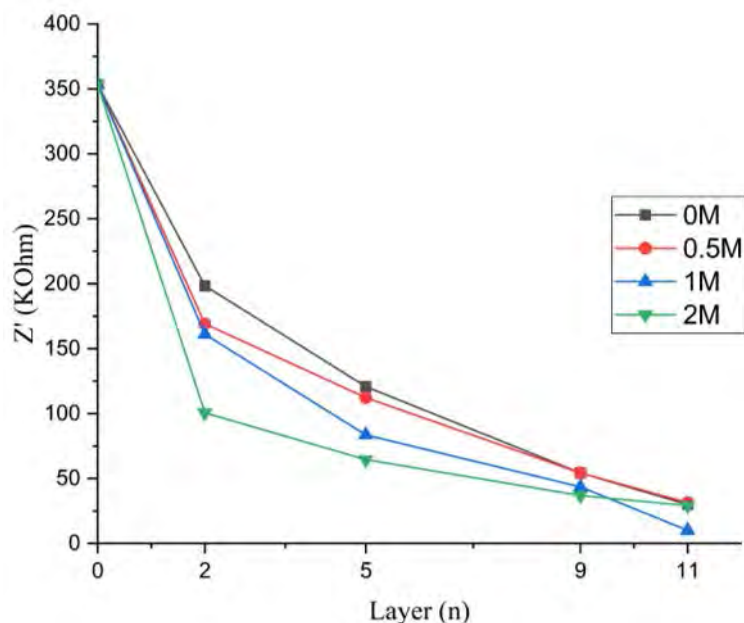
Figure 4.17. Plot of real impedance (Z') of PEMs assemblies with various concentrations of supporting electrolyte at 1kHz within increasing number of layers.

Effect of surface roughness toward the impedance result can be seen from measurement in the electrolyte solution. Assumed from this experiment that PEMs with 2M NaCl has 'loopy' structure following Decher's statement compared to other PEMs with lower concentrations of applied supporting electrolyte. So, rough surface become less conductive than smooth surface or PEMs with 'flat' structure. The resistance and or conductance of the electrode also depend on homogeneity of the surface material that correspond to the surface roughness. (Barsoukov, E., et al., 2005)

4.2.3. Effect of PEMs toward the electrode

Electrode-electrolyte interface is an interesting aspect related to impedance result. Supposed in the presence of PEMs in the interface between electrode and electrolyte either strengthen or weaken electrostatic behaviour. Hence, electrode modification by PEMs was studied in this section. PEMs were built on electrode in 2 ways, on both electrodes and on one of the electrodes as shown in **Figure 4.18**. During PEMs build up, first layer behaves like an island in between the

electrode and grow up homogeneously within number of layers assembling (Picart, C. et al., 2001).
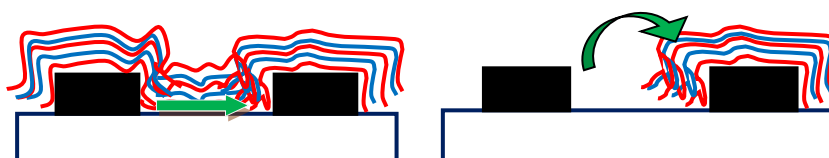
Figure 4.18. Illustration of different PEMs coating mechanism on electrode.

For all type of PEMs-coating, 2-electrodes and 1-electrode, PDAD and PSS with 1M NaCl in each solution were used to build PEMs on it by dropping mechanism. 0.6M of NaCl was used as electrolyte solution for impedance measurement. Frequency range were employed in between 20 Hz to 2 MHz and the AC level amplitude was 50 mV. Collected data then transformed into Z' (real) vs Z" (imaginary) and plotted into Nyquist plot to see the differences between layers. For single frequency measurement, data were obtained from 1 kHz.

In the electrolyte solution, the graph will appear as a semicircle connect to straight line following simple RC circuit for ideal equivalent circuit of general double layer impedance as seen in **Figure 4.19**. The semicircle is well-known as film resistant and straight line is diffusion or Warburg impedance at low frequency. The diffusion of mobile ion at low frequency is further than diffusion at high frequency. Thus, Warburg impedance will not appear at high frequencies.
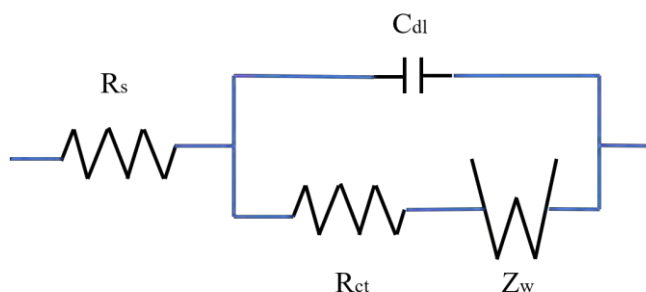
Figure 4.19. Equivalent circuit for general double-layer impedance with Warburg impedance.

Diameter of the semicircle as film resistant can be calculated from R_s and R_p, where Rs is the resistant of external factor. Because resistant Rs come from external factors, the curve was displaced to value equal to Rs in purpose for sample comparison. Capacitance of the film can be expected from the maximum frequency at Z" (imaginary) of the semicircle following equation (3) above. Where the straight line represented the diffusion of mobile ions at the electrode-electrolyte interface. Ideal equivalent circuit for AgNPs-electrode system will be discussed in the next section (4.2.5.). The angle of the straight line toward Z' (real) axis is associated to the roughness of surface at the interface.

For all type of PEMs-coating mechanism, a semicircle appeared in the frequency between 500 kHz to 1.5 MHz and below that frequency was straight line with $70°$-$80°$ angle as shown in **Figure 4.20** for coating on single electrode and **Figure 4.21** for coating on double electrodes. Both coating mechanisms had different impedance response toward increasing number of layers. When PEMs coated 2 electrodes, the semicircle diameter seemed shrinking that correspond to the decreasing of the film resistant. This decreasing was clarified with the impedance data at single frequency 1 kHz. In other hand, PEMs that coated only 1 electrode experienced widening in the semicircle diameter.
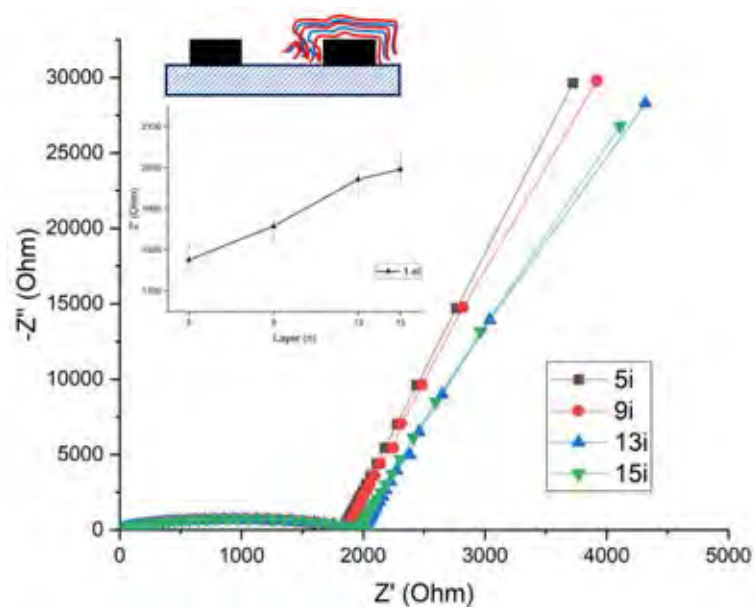
Figure 4.20. Nyquist plot of PEMs coated single electrode within increasing number of layers, inset: real impedance (Z') at 1 kHz versus number of layers.
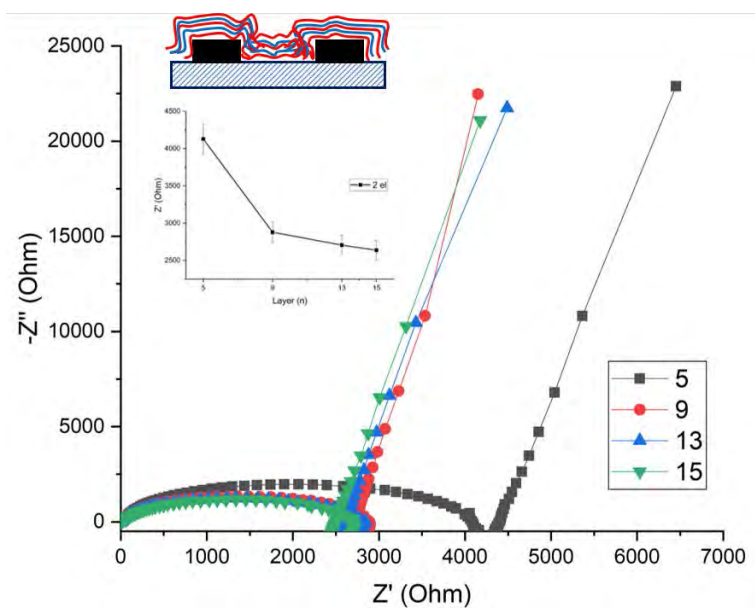
Figure 4.21. Nyquist plot of PEMs coated double electrodes within increasing number of layers, inset: real impedance (Z') at 1 kHz versus number of layers.

According to the impedance result, it seems like PEMs coated 2 electrodes created a semiconducting bridge for electric impulse to pass through from one to another electrode (Zhao et. al., 2008), whereas if only coated on 1 electrode acted as semiconducting barrier that slightly block the electric impulse to go through. This semiconducting behaviour can be caused by unpaired ion in the polymer chain or residual small ion in the adsorption process (Durstock, M. F., & Rubner, M. F., 2001).

4.2.4. Deposition AgNPs on the PEMs-modified SPE

PEMs provide charge on the surface of the electrode by the existence of excess charged ions on the outer layer. Thus, it has ability to adsorb oppositely charged molecules (Detcher, 1997). This property create ability to modify the surface of the electrode based on electrostatic attraction. In this experiment, silver nanoparticles were used to modify the surface through two modification methods, ex-situ (monolayer) and in-situ (inside). The deposition mechanism of AgNPs for both ex-situ and in-situ had been explained in the previous section about optical sensing. For being comparable, PEMs were built by assembling 15 layers of polyelectrolyte as standard substrate for both deposition mechanism.

SEM with magnification 20,000 times was used to see the surface morphology of silver nanoparticles deposition on PEMs. In **Figure 4.22**, PEMs surface without AgNPs was seen smooth and fine. AgNPs as explained above about ex-situ synthesis, were stick on the outer layer of PEMs. Afterwards, surface morphology of PEMs and the electrode changed with respect to AgNPs. Accumulation of AgNPs created rough surface looked like a rocky rugged land. The rocks made of silver nanoparticles agglomeration which still in nano-sized scale.

Meanwhile in in-situ AgNPs deposition, surface morphology was flatter than deposition by ex-situ. Even the polyelectrolyte solutions were in the same concentration, 10mM for each solution, fully ion-paired polymer chain could not be achieved in the buried part of PEMs. But, Warburg line showed low angle for in situ synthesis in the Nyquist plot as shown in **Figure 4.23**. This unique property was built as nanoreactor to fabricate polymer composite with metallic nanoparticles inside

(Joly, S., et. al., 2000). Yet, nanoparticle reaction still occurred on the surface creating a packed-rocky surface.
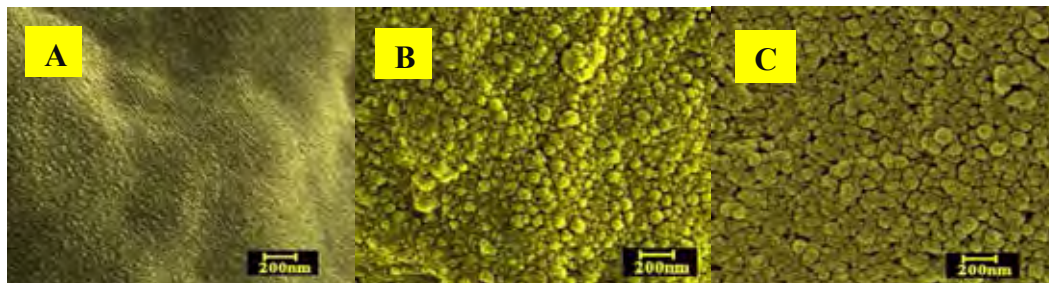
Figure 4.22. SEM images of A) PEMs 15 layers, B) Ex-situ synthesis technique of AgNPs on PEMs and C) In-situ synthesis technique of AgNPs in PEMs.
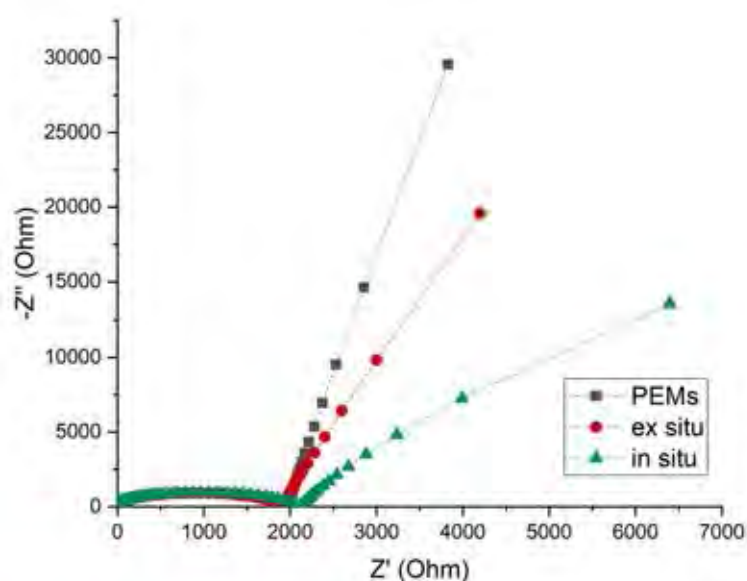
Figure 4.23. Nyquist plot of PEMs 15 layer compared to deposition of AgNPs in the electrodes through ex situ and in situ synthesis technique.

In this experiment, two coating mechanism (single and double electrode coating) combine with two silver nanoparticles synthesis technique (in situ and ex situ synthesis technique) were studied. 15 layers of PEMs were used as substrate for deposition of silver nanoparticles on electrode in all coating

mechanisms. SPE modification by different silver nanoparticles synthesis techniques were illustrated in **Figure 4.24.**
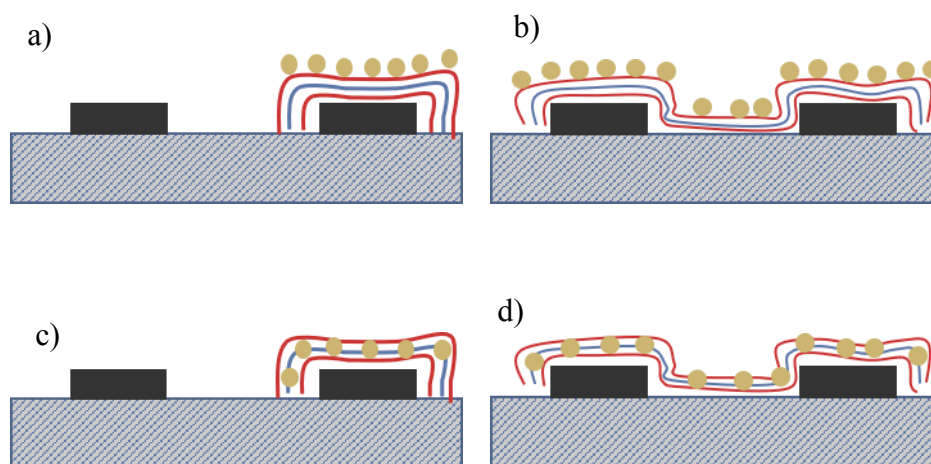
Figure 4.24. Illustration of AgNPs deposition on the electrode through; ex situ technique on a) single electrode, b) both electrodes and in situ technique on c) single electrode, d) both electrodes.

4.2.5. Equivalent Circuit Fitting

To analyze impedance result from Nyquist plot, equivalent circuit is usually used to understand the change in the system. Equivalent circuit is built from basic electrical characteristic for easy in analysis. In the impedance system, resistor, capacitor and Warburg are mostly used to represent theoretical circuit of the data. Capacitor can be substituted by Constant Phase Element (CPE) to represent nonideal capacitance behaviour. While diffusion in the system usually modelled by Warburg impedance that depicted in a semi-finite length line with θ of 45° (Barsoukov, E., et al., 2005).

For measurement in the electrolyte solution, general equivalent as shown in **Figure 4.19** can be used to simulate Nyquist plot of PEMs. But, the complexity of the experiment result that involved Warburg line in the plot which had angle larger than 45° caused a necessary to rearrange the EC circuit. After drew

several circuits and simulated with the experimental data, an equivalent circuit which can fit the experimental data was built as seen in **Figure 4.25.**
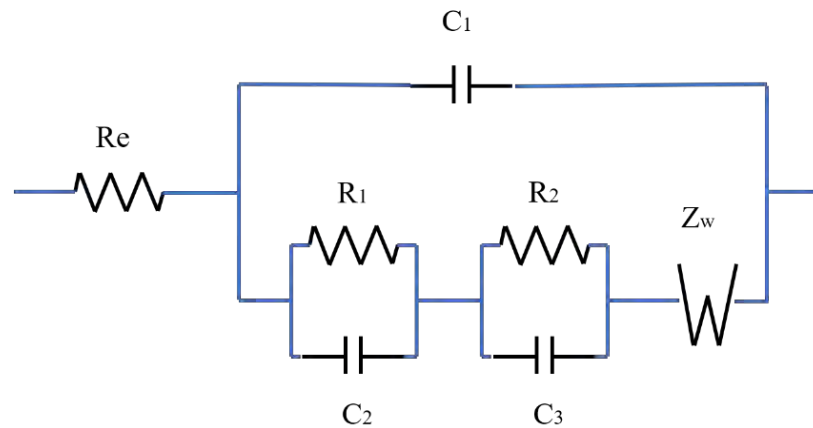
Figure 4.25. Equivalent circuit of PEMs systems which Re represent external resistance such: solution, cable and etc.

To compare with the experimental data, first step is calculating all of the component in the circuit. The calculations were done in Microsoft excel program. Warburg impedance as frequency dependent can be solved by following equation:

$$Z_w = \frac{\sigma}{\sqrt{\omega}} - j\frac{\sigma}{\sqrt{\omega}}$$

(4.2)

where σ is Warburg coefficient which include diffusion of the system, but then can be replaced by the function of admittance Y_0 (= $1/Z$) and ω is angular frequency in radians:

$$\sigma = \frac{1}{(\sqrt{2} \times Y_0)}$$

(4.3)

$$\omega = 2 \times \pi \times f$$

(4.4)

Then, basic parallel system calculation is used to solve RC model by following equation:

$$Z_p = \frac{1}{Z_r} + \frac{1}{jZ_c} = \frac{Z_r \times jZ_c}{Z_r + jZ_c}$$
(4.5)

Impedance of capacitance is added by 'j' that correspond to imaginary number ($j : -1^{1/2}$) and also a function of frequency as shown bellow:

$$jZ_c = \frac{1}{j \times 2 \times \pi \times f \times C}$$
(4.6)

After solving the parallel unit, both units behave as series model and combine by basic series system calculation as follow:

$$Z_s = Z_r + jZ_c = \sqrt{Z_r{}^2 + jZ_c{}^2}$$
(4.7)

Z total that obtain from the combination of two parallel RC system then added to Warburg impedance by equation (4.7) and combine with the capacitance of double layer (C_1) by equation (4.5). Here, R_e can be ignored from the system because this is the resistance of external factors. Angle of each frequency can be obtained by following equation:

$$\theta = \tan^{-1}\left(\frac{-jZ_c}{Z_r}\right)$$
(4.8)

From the equations above, this equivalent circuit result then compared to the experimental data of AgNPs coated electrode by in situ synthesis mechanism in the frequency range of 20 Hz – 2 MHz. The comparison graph is shown in **Figure 4.26** that this proposed EC almost fit with the experimental data, even though for the experiment result contains complexity. In the low frequency

range, can be seen a small widen of the Warburg line at 40Hz-100Hz but then merge again in the frequency above that. By using this proposed EC, angle of Warburg is satisfying.

Different PEMs coating and silver nanoparticles synthesis for each coating method were also fitted with this equivalent circuit. Although problem was found at low frequency as mentioned before, overlapped semicircle at high frequency was well fitted. All fitting graph can be seen at Appendix C.
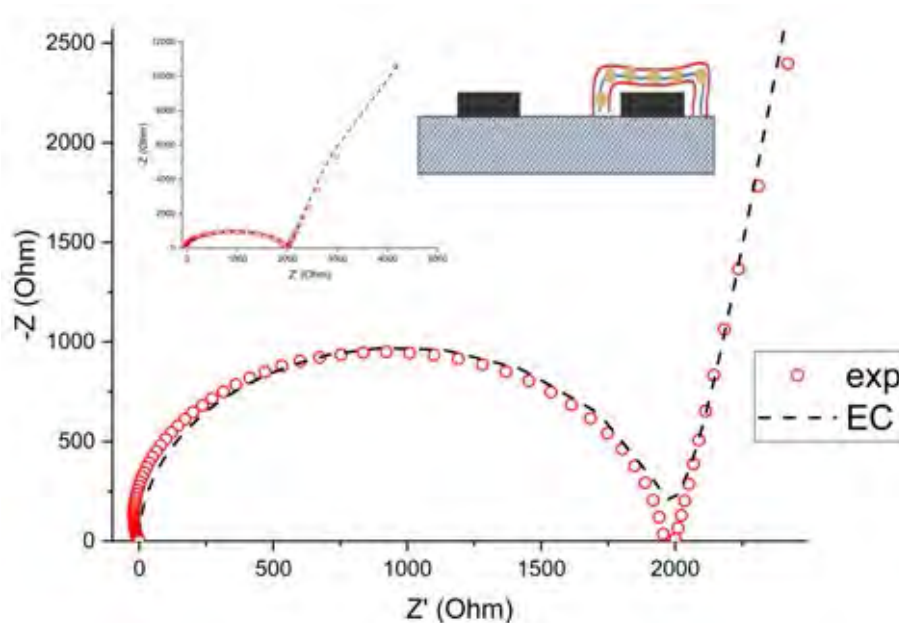
Figure 4.26. Comparison graph of experimental data result from AgNPs-PEMs coated single electrode by in situ synthesis technique versus the equivalent circuit.

From this proposed equivalent circuit, the experimental result can be analized on why the Warburg line was ended with semicircle that come from capacitance characteristics. Based on Warburg impedance and capacitance impedance that act as frequency-dependent elements from equation (4.2) and (4.6) respectively, a given value of both elements experience a decreasing with the increasing of frequency. Since this equivalent circuit is a parallel system and both elements stand in different line the calculate the value by using equation 4.2 and 4.6 with the same applied frequency of experiment set up. The value will be the opposite

and if plotted in one graph will intersect at certain frequency as seen from **Figure 4.27**. at low frequency, Warburg has high value but then decrease within the increasing of applied frequencies. Researches correlated Warburg impedance to diffusion characteristic. Diffusion of the ion on the substrate is the cause of obtaining angle. So, Warburg is defined as diffusion path length and limited by particle size. At high frequency, diffusion path length is less than available region for diffusion (Barsoukov, E., et al., 2005).
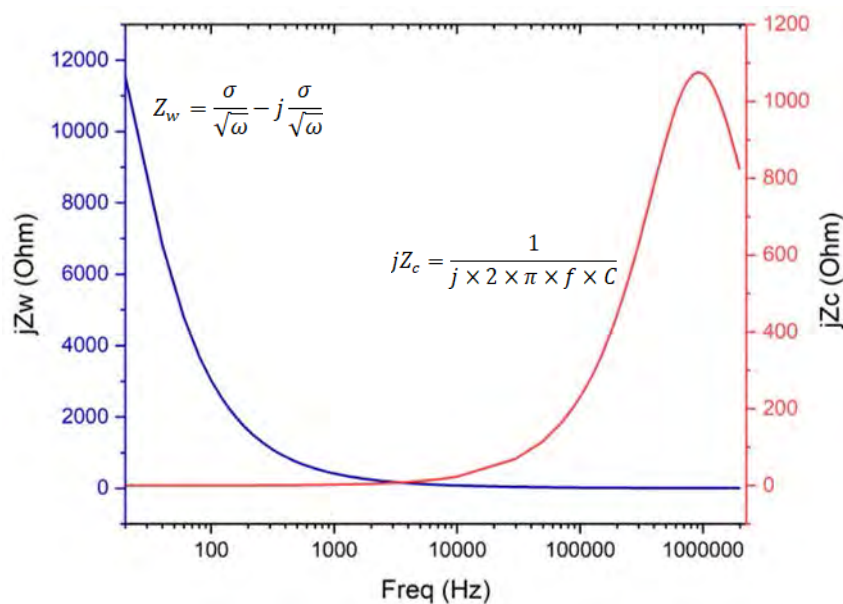
Figure 4.27. Warburg impedance (jZw) vs capacitance impedance (jZc) with applied frequencies.

Within low frequency, diffusion impedance is taking place (jZw > jZc) till at point where diffusion is limited due to high frequency and jZw = jZc. Capacitance start to take over the entire system (jZc > jZw) at frequency about 5 kHz. From the graph above, capacitance at low frequency is very low (jZc < jZw) and increase by the increasing of frequency till maximum point which is called by maximum frequency (f_{max} about 900 kHz for this sample) and then will decrease. This simulation can give information about the termination of Warburg line by semicircle in the term of frequency effect.

4.2.6. Application of Equivalent Circuit

Equivalent circuit is assumed to represent electrical elements in the tested sample. Therefore, elements in the drawn EC need to be proven by experimental data. For comparison, nyquist plot from experimental data will be plotted next to nyquist plot from EC with same applied frequency. Succesfull comparison is indicated by overlaping plot of the graph from both subjects.

First is in the low frequency region, which is Warburg impedance. Many researches agreed that Warburg is corresponded to the diffusion of ion in the system. It is quite hard to discuss about diffusion of ion in the system. Another assumption said that Warburg is about diffusion path length in low frequency region. Low frequency generates wide path of ion for move. With increasing frequency which is the movement of ion become faster, then at certain frequency the ion will not move at all because of the applied frequency is too fast.

The diffusion path length of ion then assumed to be an active area in the proposed EC system. Active area is located in the surface of the system. Then, larger active area at certain dimensions means that the surface of the system is more rough than other system which has lower active area at same dimensions. To strengthen this assumption, annealed PEMs with 15 layers was compared to non-annealed PEMs. Annealing was done by using 2 M NaCl for 30 minutes. This mechanism will draw some water ion and smooth PEMs surface (Dubas, S. T., 2001) as seen from the AFM result in **Figure 4.28.** SEM was used to see the difference in surface roughness of both samples.
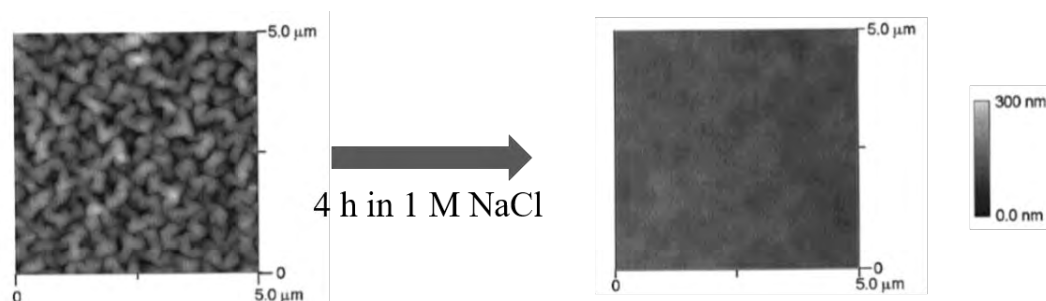
Figure 4.28. AFM image of PEMs before and after annealing in 1 M NaCl for 4 hours. (Dubas, S.T., 2001)

Impedance result show difference at the Warburg line as predicted before. The annealed PEMs had nice spike which was straight and higher angle than non-annealed PEMs. The difference occurred at low frequency about 20 Hz to 200 Hz as seen in **Figure 4.29**. While at high frequency almost found no differences. The semicircles were overlapped each other means that the annealing mechanism will not affect those high frequencies region. The SEM images verified the distribution of surface roughness for both samples.
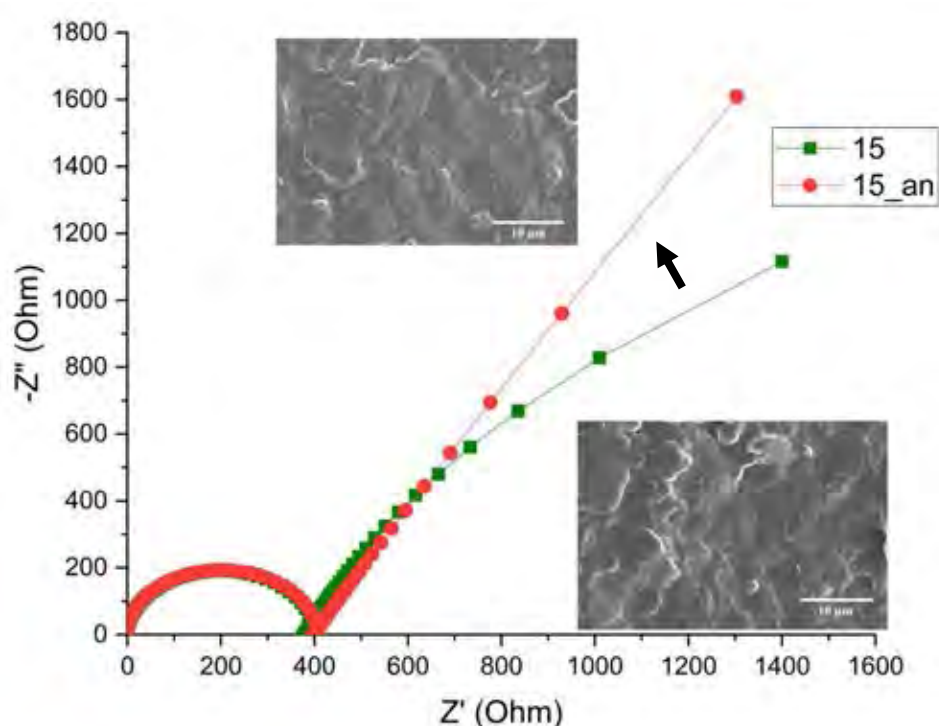
Figure 4.29. Nyquist plot of annealed PEMs with 15 layers and non-annealed PEMs, inset : SEM images of annealed and non-annealed PEMs.

In the presence of silver nanoparticles on the PEMs coated electrode, the angle of Warburg line also decrease. From experimental data, in situ AgNPs synthesis has smaller angle than ex situ and pure PEMs meaning that in situ has rough surface among others. Ability of in situ synthesis technique to deposit AgNPs inside of PEMs is considered to create larger active surface area. And it slightly no change in the diameter of semicircle at high frequency. In the EC, the angle come

from combination of Z_w, R_2 and C_3. Z_w and R_2 are used to adjust the angle of the straight line and C_3 is used to adjust the length of the tail at low frequency. From these characteristics, R_2 and C_3 can be committed to represent the electric element in the silver nanoparticles layer.

Next part is high frequency regions. As known before that at these regions yield semicircle in the Nyquist plot centered on the real axis which represent capacitive behaviour of the system (Barsoukov, E., et al., 2005). The semicircle is obtained from the combination of R and C element in parallel system. It was hypothesized that the main cause is electrode-electrolyte interface. Several variables were used to study the system at high frequency regions such as: number of layers, various concentration of electrolyte solution, various kind of salts and different kind of electrodes.

Relation between number of layers and coating mechanism are discussed above which coating on single electrode behave as semiconducting barrier layer and coating on both electrodes behave as semiconducting bridge. For semiconducting barrier property, diameter of semicircle will increase with increasing number of layers. Addition of layers will strengthen the blocking behaviour of the electric impulse or increase the resistance of the system. While semiconducting bridge creates path for electric impulse to move from one to other electrode and thus will decrease the resistance or decrease semicircle diameter.

Beside testing internal factor, external factor become another concern to study. PEMs coated electrode were then tested with different electrolyte solution to see any effect to the collected data. Various concentration of NaCl were used for electrolyte from 0 M to 0.01M. in the higher salt concentration, the semicircle seemed decreasing in diameter. This may be caused by number of containing ion in the electrolyte solution which effects the diffusion or help the transfer of electric impulse. Then NaCl were substituted by other salt species (CH_3COONa and KCl) for the same test mechanism, and same result were obtained. In term of strong electrolyte, within the same electrolyte concentration measurement, measurement in the NaCl showing the smallest semicircle diameter among others two utilized salts in this experiment as shown in **Figure 4.30**.
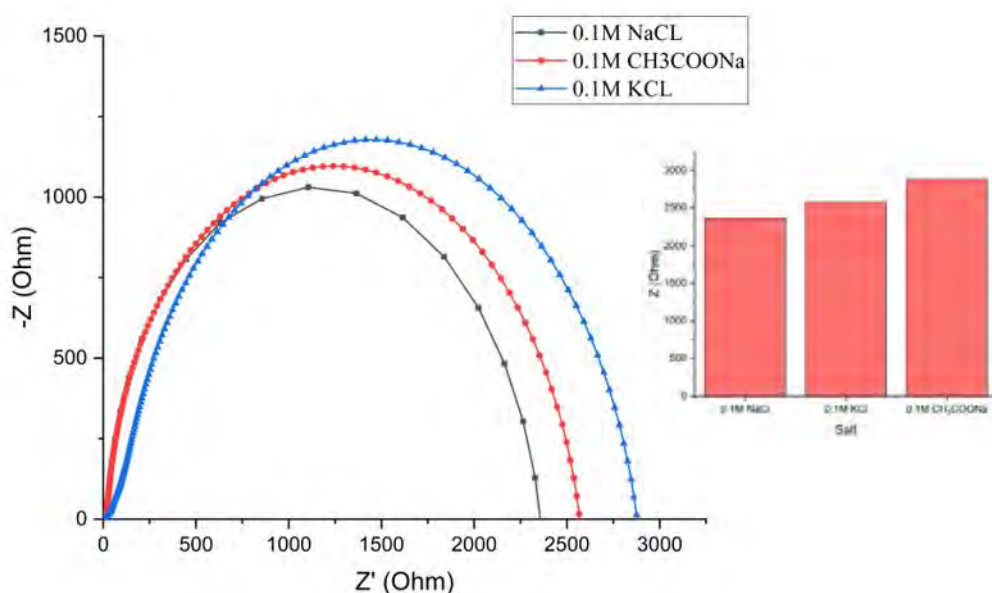
Figure 4.30. Nyquist plot of PEMs measured in 0.1M NaCL, 0.1M CH$_3$COONa and 0.1M KCl at high frequencies range. Inset: diagram of semicircle diameter.

Different kind of electrode also were tested. Carbon-SPE and silver-SPE which made by different electrode species produce different semicircle diameter in the Nyquist plot. In term of resistivity, carbon has higher resistivity than silver about 2.5 x 10^{-6} Ωm and 1.59 x 10^{-8} Ωm for each respectively. Thus, this electrical property affect the impedance result by small diameter about 200 Ω for silver electrode compare to 2000 Ω for carbon electrode .

From testing experiment above, almost all variables were affecting the Nyquist plot at high frequency regions in term of semicircle diameter. Moreover, different kind of electrode material had significant change in resistance. Then, the semicircle is fully focused to the interface of electrode-electrolyte. This film property can be represented by R$_1$ and C$_2$ which stand in parallel line as film resistance and capacitance respectively. R1 is used to adjust the diameter of semicircle. While C$_1$ and C$_2$ are used to adjust the curve to create nice semicircle. C$_1$ can be assumed to represent whole capacitance of the composite film. The combination of low and high frequency then applied to the AgNPs-PEMs-electrode system as seen in **Figure 4.31.**
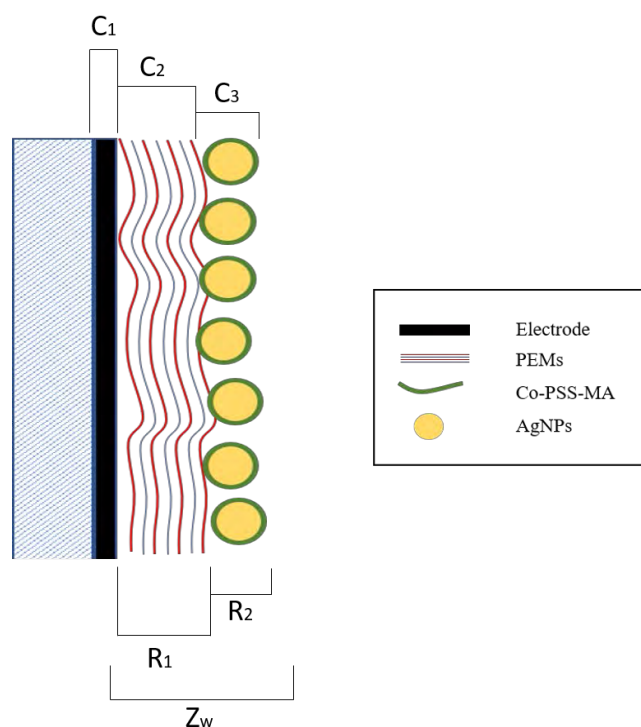
Figure 4.31. Application of EC to the AgNPs-PEMs-electrode system

4.2.7. H₂S Gas Sensing

H_2S is a toxic compound in the environment which form in gas phase. H_2S gas was generated from chemical reaction between Na2S and hydrochloric acid in solution following double replacement chemical reaction bellow;

$$Na_2S_{(aq)} + 2\ HCl_{(aq)} \quad \rightarrow \quad H_2S_{(g)} + 2\ NaCl_{(aq)} \qquad (4.9)$$

The reaction occurs because both reactants exchange cation and anion and yield new product. To produce 100% yield of H_2S gas, excess of HCl was used in this reaction experiment. Indication of the formation of H_2S gas from this reaction is a presence of rotten egg smell from the reaction chamber. Also, when this chamber was connected to another chamber that contain $CuSO_4$ and let the gas pass through, black precipitate appeared in the $CuSO_4$ solution. Black precipitate is CuS as yield

from the reaction. This can be an evidence of H_2S gas formation from previous chamber.

AgNPs coated electrode through two different synthesis and coating mechanisms were placed in the chamber and connected to gas reaction chamber with excess HCl and leave for overnight. Approximately 100 ppm of H_2S gas were formed for 100% yield were used for first experiment. EIS result before and after exposure were compared through Nyquist plot. In the optical sensing part, sulfidation in the membrane will degrade AgNPs layer that can change the absorbance spectra. SEM was used to see how sulfidation affected the AgNPs on the electrode. The degradation then compared with soaking AgNPs coated electrode in 1% H_2O_2 solution.

4.2.7.1. Reaction kinetics analysis using EIS

To understand the sensitivity of the silver nanoparticles toward sulfide ion, reaction kinetics form various concentration of sulfide ion were used to analyze. Instead of using H2S gas which difficult to determine the concentration, Na_2S from solid material was used for this experiments. By using Na_2S, concentration in the solution can be determined easily by weight.

Solid Na_2S were disolved in DI water. Concentrations of Na2S were varied from 400 ppm, 40 ppm, 4 ppm and 400 ppb. For this experiment, AgNPs were synthesised on the electrode through in situ synthesis technique on both electrodes. Measurement were done in DI water for each collected data in one hour. Frequencies swept between 20 Hz to 2 MHz. Each collected data for each concentration are shown in **Figure 4.32.**

Measurement in DI water has bigger diameter of semicircle than measurement in the electrolyte solution as discussed before. Each measurement in each concentration experienced increasing at the semicircle diameter. For 400 ppm and 40 ppm, the diameters widening were significant from first 15 minutes and slightly change after that. But in the last 15 minutes, imaginary impedance peaks were decreasing for both concentrations. This indicate a change in the film capacitance.
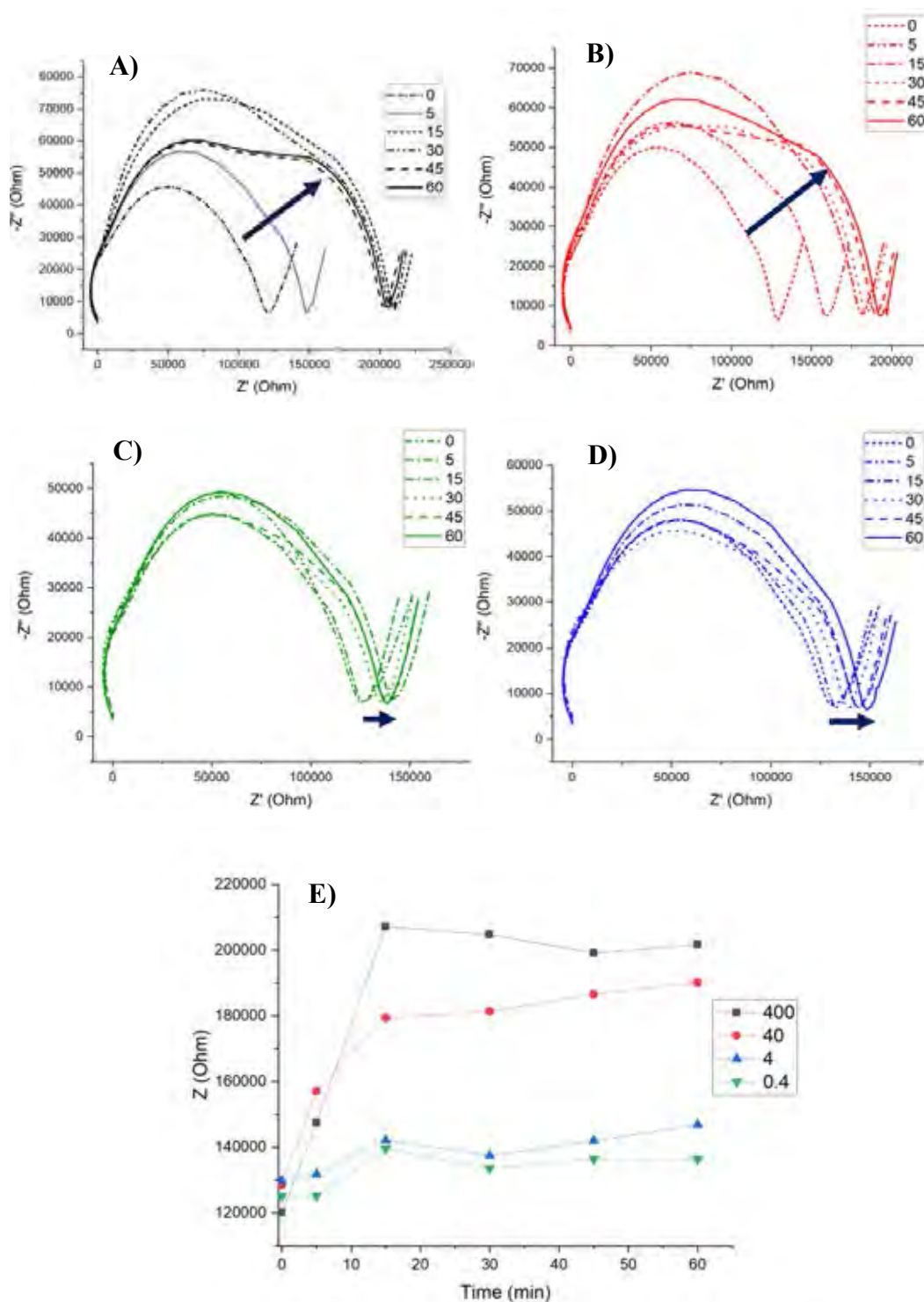
Figure 4.32. Nyquist plot of AgNPs in electrode through in situ synthesis technique toward various concentrations of Sulfide ion, A) 400 ppm, B) 40 ppm, C) 4 ppm and D) 400 ppb, and E) Plot of impedance at 1 kHz versus time.

For another two low concentrations, 4 ppm and 400 ppb, semicircle diameter didn't experience significant change but still occurred. In the summary of the measurement by taking 1 kHz as comparison, the differences in the impedance change were cleary seen. It seemed reaction go fast for first 15 minutes and slown down after that. 400 ppb has lowest change in impedance but still can be detected by using electrochemical impedance spectroscopy.

4.2.7.2. H_2S Sensing

The sulfidation of AgNPs will induce aggregation of the nanoparticles (Schlich, K. et al., 2018). The aggregation was seen in ex situ synthesis mechanism where bulk nanoparticles more than 200 nm in size were created after exposure. While for in situ synthesis, some holes were appeared that might cause by sulfidation. The holes were predicted from silver nanoparticles that attracted from the film because in situ synthesis will deposit nanoparticle inside the film. Sulfide will interact with silver nanoparticles in the surface and create Ag_2S and then induce aggregation of silver nanoparticles at surrounding area. SEM images for before and after measurement are shown in **Figure 4.33.**
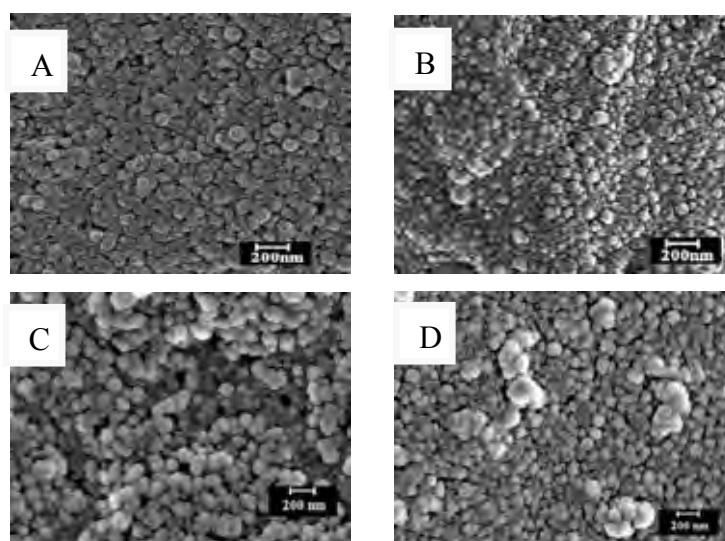
Figure 4.33. SEM images before exposure of AgNPs electrode to H_2S of A) In situ B) Ex situ synthesis mechanism and after exposure C) & D) for each respectively.

10 ppm and 100 ppb of H2S gas were used to test the sensitivity of AgNPs coated electrode. In situ synthesis of silver nanoparticles on single electrode had better sensitivity among other samples for sensing 10 ppm H_2S gas followed by ex situ synthesis on both electrodes as seen in **Figure 4.34.** The graphs were based on change of film resistance after exposure. 17% change in semicircle diameter and also Warburg line which become straighter than before exposure. Aggregation of Ag_2S might decrease surface active area of the composite film then Warburg line behave like a smooth surface. At 100 ppb H_2S gas sensing, almost all sample experienced 3% in semicircle diameter decreasing except for ex situ silver nanoparticles synthesis on substrate on single electrode.

As discussed above that coating on single electrode behave like a semiconducting barrier. In the presence of silver nanoparticles will strengthen the blocking behaviour. Although silver nanoparticles were deposited inside the composite as filler through in situ synthesis mechanism, electric impulse still feel blocking properties. This become a question on why in the presence of silver nanoparticles as filler will not decrease the resistance of the composite. But after being exposed to H_2S gas which reacted some silver nanoparticles to be Ag_2S, the composite resistance decreased.

The decreasing of composite film resistance between in situ synthesis technique and ex situ synthesis technique after being exposed lead to the reactivity of silver nanoparticles toward H_2S gas. And even in the presence of small amount of the gas in ppb, the impedance results still show differences. Higher change for in situ than ex situ might understandable because in the loss of silver nanoparticles from inside will also remove blocking element from electric impulse pathway where for ex situ, silver nanoparticles on outer layer, the blocking element not in the pathway exactly. Both synthesis mechanism showed blocking electric impulse because the film thickness only in nanoscale which might be not thick enough to separate between electrode and outer layer of the PEMs.
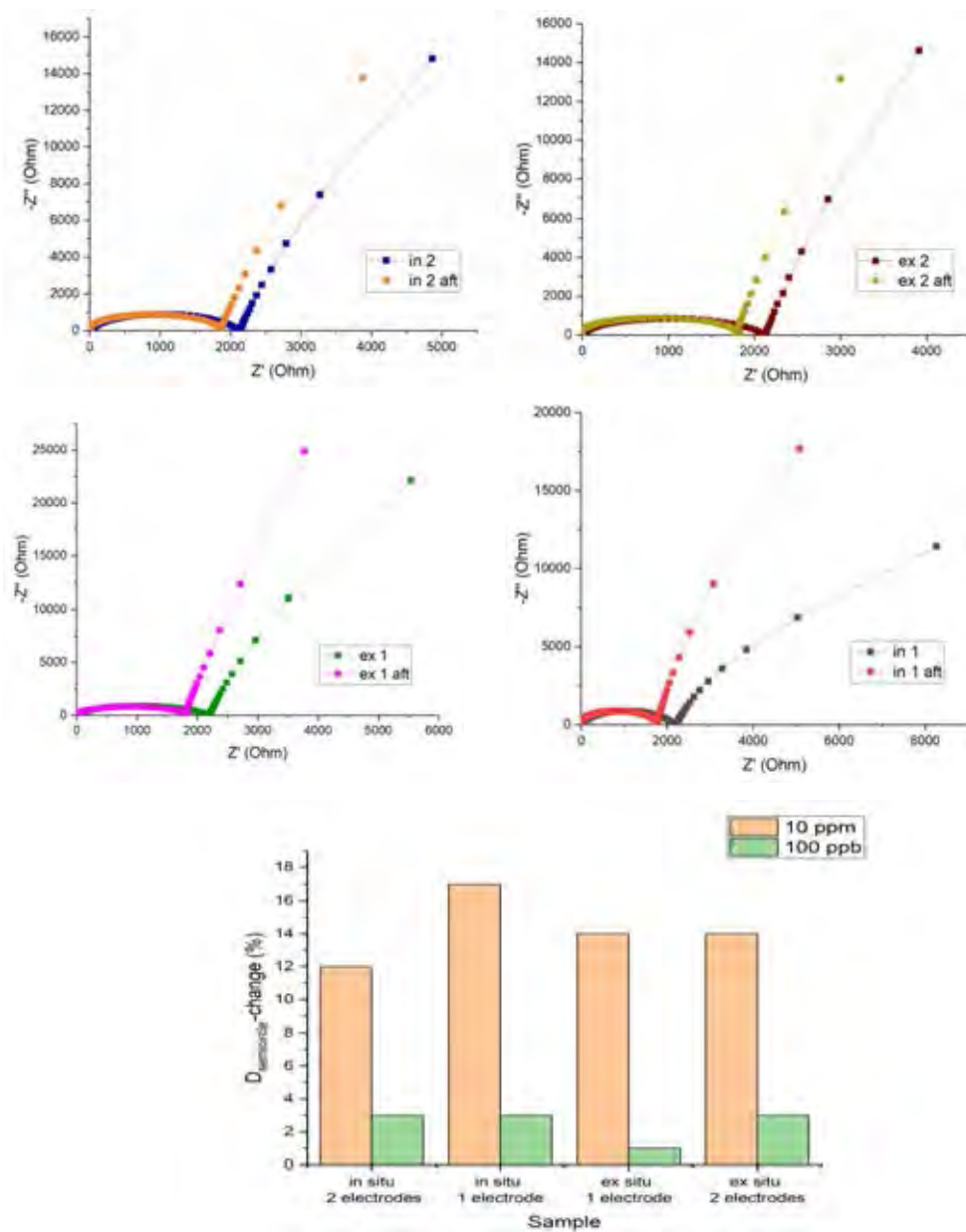
Figure 4.34. Nyquist plot of before and after exposure of 10 ppm H2S gas for each electrode and plot of diameter change after exposure of H2S gas for 10 ppm and 100 ppb.

The Nyquist plot of experimental data were fitted with the equivalent circuit in Figure 4.12 and compared for further analysis. Value of EC elements were placed in **Table 4.1.** for easiness in comparison. All sample experienced a decreasing in film resistance (R_1) and almost no significant differences in film capacitance (C_2).

Something unique was that all of R_2 in the sample increased after exposure. If in the discussion before (section 4.2.6) assumed that R_2 correspond to the nanoparticles resistance, this phenomenon showed the disappearance of silver nanoparticle in the composite film and become Ag_2S. Thus, R_2 represent remaining silver nanoparticles that unracted with H_2S gas. The increasing of spike angle for all sample after exposure were proven the statement about silver nanoparticles and decreasing the surface active area.

Table 4.1. Result of fitting the experimental data of Nyquist plot of before and after being exposed to 10 ppm H_2S gas to equivalent circuit as in **Figure 4.25**

	Before being exposed to 10 ppm H_2S gas			
	In situ tech 1 electrode	Ex situ tech 1 electrode	In situ tech 2 electrodes	Ex situ tech 2 electrodes
R1 (Ω)	2150	2125	2100	2100
R2 (Ω)	27000	180000	100000	160000
C1 (F)	4E-10	5E-10	5E-10	3E-10
C2 (F)	8E-11	8E-11	9E-11	9E-11
C3 (F)	6.3E-07	3.7E-07	5.6E-07	5.7E-07
Aw (Ω s$^{-1/2}$)	13000	10000	9000	7000
Θ (º)	62.17	81.17	79.25	82.76
	After being exposed to 10 ppm H_2S gas			
	In situ tech 1 electrode	Ex situ tech 1 electrode	In situ tech 2 electrodes	Ex situ tech 2 electrodes
R1 (Ω)	1780	1830	1850	1800
R2 (Ω)	110000	450000	130000	250000
C1 (F)	1E-09	4E-10	9E-10	8E-10
C2 (F)	9E-11	9E-11	8E-11	9E-11
C3 (F)	4.5E-07	3.3E-07	5.8E-07	6.5E-07
Aw (Ω s$^{-1/2}$)	7000	8000	7000	7000
Θ (º)	79.24	85.39	81.78	84.58

4.2.8. <u>Sensing Frequency</u>

For easiness and simplicity in the application of sensing device, applied frequency is needed to be specify. For this purpose, bode plot of experimental data of in situ silver nanoparticles synthesis in single electrode between before and after being exposed to H_2S gas was used. In the bode plot, frequency is used as x-axis and in this plot imaginary impedance (-Z") is used as y-axis as seen in **Figure 4.35.** The result difference was seen significant at frequency 20 Hz compared to 1 MHz. This might be caused by a change in the surface area either the roughness or surface active area. From the **Figure 4.27** was discussed about Warburg impedance is dominant at low frequency (jZw > jZc) that correspond to the tilt of the angle and capacitance dominates at high frequency (jZc > jZw) that correspond to semicircle diameter.
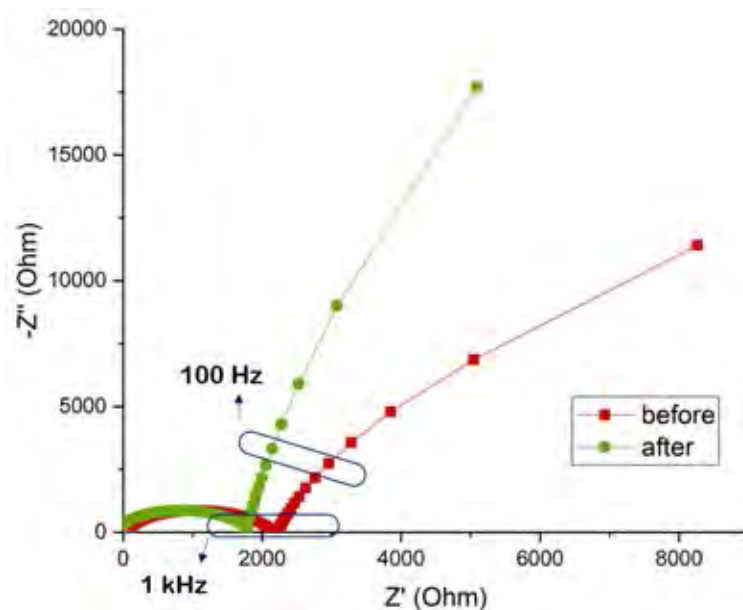
Figure 4.35. Nyquist plot of before and after sensing of 10 ppm by using AgNPs through in situ synthesis technique on 1 electrode and frequency plot at 100 Hz and 1 kHz.

Available impedance portable device in the market provide test frequency options between 100 Hz to 200 kHz. From the experimental data, that

frequency range is still include in sensitive range for impedance sensing. Direct impedance data (Z) change between before and after exposure of H_2S gas in percentage were placed in **Table 4.2.** Test frequency at 100 Hz showed high sensitivity followed by 1 kHz and 100 kHz. And modification of electrode by silver nanoparticles through in situ synthesis technique has better sensitivity among other methods. Based on this result, the modified electrode can be used to be a H_2S gas sensing in portable device.

Table 4.2. Direct impedance result change between before and after exposure of H_2S gas on various modified electrode.

Sample \ Freq	100 Hz	1 kHz	10 kHz	100 kHz
Ex situ 1 electrode	3.23%	0.27%	0.75%	0.89%
Ex situ 2 electrodes	5.01%	0.74%	0.45%	0.17%
In situ 1 electrode	3.83%	2.48%	2.33%	2.57%
In situ 2 electrodes	3.86%	1.86%	2.21%	2.47%

CHAPTER V
CONCLUSSION AND RECOMENDATION

In the optical sensing, well capped silver nanoparticles in the solution showed satisfying result for sulfide ion sensing due to its size and optical properties. While, Ex situ synthesis technique had significant change in absorbance than in situ synthesis technique. Absorbance spectra for ex situ synthesis technique were increasing and in situ absorbance spectra were decreasing after exposure. Then can be conclude that AgNPs as monolayer were more exposable to sulfide ion than as a filler.

In purpose of impedance sensing, modification of screen printed electrode can be achieved by using PEMs as substrate to deposit silver nanoparticles. PEMs coating electrode has different behaviour for different coating mechanism either single electrode coating or double electrode coating. Single coating electrode behave a semiconducting barrier where double coating electrode behave a semiconducting bridge. And within the deposition of silver nanoparticles either monolayer on top or filler inside the film, impedance result showed change in warburg line that correspond to surface roughness or surface active area.

Equivalent circuit as shown in **Figure 4.25** can be fitted with experimental datas and used for further analysis. Electric element in the equivalent circuit were assumed to represent sample elements. R1 represent film resistance and R2 represent nanoparticles resistance. C2 represent film capacitance, C3 represent nanoparticles capacitance and C1 represent whole system capacitance. Zw represent surface active area or surface roughness of the sample.

For H_2S gas sensing, modification of the electrode by silver nanoparticles through in situ synthesis technique gave better sensitivity among other methods. This might be caused by the silver nanoparticles as filler that had direct dealing with electric current than monolayer on top (ex situ technique). In specifying of testing frequency, applied frequency for measurement were compared to provided frequency by portable LCR analyzer in the market. Thus, available test frequencies in the market still include in sensitive frequency range in the experimental data. So, further testing and studying are necessaries to build the portable impedance gas sensor device.

REFERENCES

AMAP/UNEP. (2013) <u>Technical Background Report for the Global Mercury Assessment 2013.</u> Arctic Monitoring and Assessment Programme, Oslo, Norway/UNEP Chemicals Branch, Geneva, Switzerland. vi + 263 pp.

Annadhasan, M., Muthukumarasamyvel, T., Babu, V.R.S., and Rajendiran, N. (2014). Green synthesized silver and gold nanoparticles for colorimetric detection of Hg^{2+}, Pb^{2+}, and Mn^{2+} in aqueous medium. <u>Sustainable Chemistry & Engineering</u>, 2, 887-896.

Baalousha, M., Arkill, K. P., Romer, I., Palmer, R. E., & Lead, J. R. (2015). Transformations of citrate and Tween coated silver nanoparticles reacted with Na2S. <u>Science of the Total Environment</u>, 502, 344-353

Barsoukov, E. (2005). Impedance Spectroscopy Theory, Experiment, and Applications Second Edition Preface. Impedance Spectroscopy: Theory, Experiment, and Applications, 2nd Edition, Xii-+.

Cabassi, J., Tassi, F., Venturi, S., Calabrese, S., Caphecciacci, F., D'Alesandro, W. and Vaseli, O. (2017). A new approach for the measurement of gaseous elemental mercury (GEM) and H2S in air from anthropogenic and natural sources: examples from Mt. Amiata (Siena, Central Italy) and Solfatara Crater (Campi Flegrei, Southern Italy). <u>Geochemical Exploration</u>, 174, 48-58

Daware, K., Shinde, R., Kalubarme, R.S., Kasture, M., Pandey, A., Terashima, C., and Gosavi, S.W. (2018). Development of optical sensing probe for Hg(II) ions detection in ground water using Au, Hexanedithiol and Rhodamine B nanocomposite system. <u>Sensor and Actuators B: Chemical,</u> 265, 547-555.

Decher, G. (1997). Fuzzy nanoassemblies: Toward layered polymeric multicomposites. <u>Science,</u> 277(5330), 1232-1237.

Decher, G. and Schmitt, J. (1992). Fine-Tuning of the film thickness of ultrathin multilayer films composed of consecutively alternating layers of anionic and cationic polyelectrolytes. <u>Progr Colloid Polym Sci</u> 89:160-164.

Deiseroth, H. J. (1997). Alkali metal amalgams, a group of unusual alloys. <u>Progress in Solid State Chemistry</u>, 25(1-2), 73-123.

Detsri, E. (2016). Novel colorimetric sensor for mercury (II) based on layer-by-layer assembly of unmodified silver triangular nanoplates. <u>Chinese Chemical Letters</u>, 27(10), 1635-1640.

Dubas, S. T., & Schlenoff, J. B. (2001). Swelling and smoothing of polyelectrolyte multilayers by salt. <u>Langmuir,</u> 17(25), 7725-7727.

Dubas, S. T., Wacharanad, S., & Potiyaraj, P. (2011). Tunning of the antimicrobial activity of surgical sutures coated with silver nanoparticles. Colloids and Surfaces a-Physicochemical and Engineering Aspects, 380(1-3), 25-28

Durstock, M. F., & Rubner, M. F. (2001). Dielectric properties of polyelectrolyte multilayers. Langmuir, 17(25), 7865-7872.

El-Fekky, A.A., El-Azab, W., Ebiad, M.A., Masod, M.B., and Faramay, S. (2018). Monitoring of elemental mercury in ambient air around an Egyptian natural gas processing plant. Natural Gas Science and Engineering, 54, 189-201.

European Community. (2002). Ambient Air Pollution by Mercury (Hg). Belgium: EU Agency

Evanoff, D. D., & Chumanov, G. (2005). Synthesis and optical properties of silver nanoparticles and arrays. Chemphyschem, 6(7), 1221-1231

Fares, H. M., & Schlenoff, J. B. (2017). Diffusion of Sites versus Polymers in Polyelectrolyte Complexes and Multilayers. Journal of the American Chemical Society, 139(41), 14656-14667

Fletcher, N. D., Lieb, H. C., & Mullaugh, K. M. (2019). Stability of silver nanoparticle sulfidation products. *Science of the Total Environment, 648*, 854-860.

Gonzalez-Raymat, H., Liu, G. L., Liriano, C., Li, Y. B., Yin, Y. G., Shi, J. B., . . . Cai, Y. (2017). Elemental mercury: Its unique properties affect its behavior and fate in the environment. Environmental Pollution, 229, 69-86.

Grabar, K. C., Freeman, R. G., Hommer, M. B., & Natan, M. J. (1995). Preparation and Characterization of Au Colloid Monolayers. Analytical Chemistry, 67(4), 735-743.

Han, K.N., Choi, J., and Kwon, J. (2017). Gold nanozyme-based paper chip for colorimetric detection of mercury ions. Scientific Reports, 7, 2806.

Hasanjani, H.R.A. (2019). An electrochemical sensor for attomolar determination of mercury(II) using DNA/poly-L-methionine-gold nanoparticles/pencil graphite electrode. Biosensors and Bioelectronics, 128, 1-8

Joly, S., Kane, R., Radzilowski, L., Wang, T., Wu, A., Cohen, R. E., . . . Rubner, M. F. (2000). Multilayer nanoreactors for metallic and semiconducting particles. Langmuir, 16(3), 1354-1359.

Kailasa, S.K., Chandel, M., Metha, V., and Park, T.J. (2018). Influence of ligand chemistry on silver nanoparticles for colorimetric detection of Cr3+ and Hg2+ ions. Spectrochimica Acta Part A: Molecular and Biomolecular Spectroscopy, 195, 120-127

Limsavarn, L., Sritaveesinsub, V., & Dubas, S. T. (2007). Polyelectrolyte assisted silver nanoparticles synthesis and thin film formation. Materials Letters, 61(14-15), 3048-3051.

Lin Si, and Ariya, P.A. (2018). Review: recent advances in atmospheric chemistry of mercury. Atmosphere, 9, 76

Lvov, Y., Decher, G., & Mohwald, H. (1993). Assembly, Structural Characterization, and Thermal-Behavior of Layer-by-Layer Deposited Ultrathin Films of Poly(Vinyl Sulfate) and Poly(Allylamine). Langmuir, 9(2), 481-486.

Marumoto, K., Sudo, Y., and Nagamatsu, Y. (2017) Collateral variations between the concentrations of mercury and other water soluble ions in volcanic ash samples and volcanic activity during the 2014-2016 eruptive episodes at Aso volcano, Japan. Journal of Volcanology and Geothermal Research, 341, 149-157.

Mansfeld, F (1999). *Solartron,* Los Angeles, CA, USA

Occupational Safety and Health Administration (OSHA), Hydrogen sulfide standard, 6 November 2019, <https://www.osha.gov/SLTC/hydrogensulfide/standards.html>

Pandey, S. K., Kim, K. H., & Tang, K. T. (2012). A review of sensor-based methods for monitoring hydrogen sulfide. Trac-Trends in Analytical Chemistry, 32, 87-99.

Pham, T.T.B., Junpen, A., and Garivait, S. (2015) An investigation of atmospheric mercury from power sector in Thailand. Atmosphere, 6, 490-502.

Picart, C., Lavalle, P., Hubert, P., Cuisinier, F. J. G., Decher, G., Schaaf, P., & Voegel, J. C. (2001). Buildup mechanism for poly(L-lysine)/hyaluronic acid films onto a solid surface. Langmuir, 17(23), 7414-7424

Poste, A.E., Pastukhov, M.V., Braaten, H.F.V., Ozersky, T., and Moore, M. (2018). Past and present mercury accumulation in the Lake Baikal Seal: temporal trends, effect of life history,a and toxicological implications. Environmental Toxicology, 37(5), 1476-1486.

Rex, M., Hernandez, F. E., & Campiglia, A. D. (2006). Pushing the limits of mercury sensors with gold nanorods. Analytical Chemistry, 78(2), 445-451.

Sharma, P., Mourya, M., Choudhary, D., Goswami, M., Kundu, I., Dobhal, M.P., Tripathi, C.S.P., and Guin, D. (2018). Thiol terminated chitosan capped silver nanoparticles for sensitive and selective detection of mercury(II) ions in water. Sensor and Actuators B, 268, 310-318.

Schroeder, W.H., and Munthe, J. (1998). Atmospheric mercury-an overview. Atmospheric Environment, 32(5), 809-822.

Steffen, A., Douglas, T., Amyot, M., Ariya, P., Aspmo, K., Berg, T., Bottenheim, J., Brooks, S., Cobbett, F., Dastoor, A., Dommergue, A., Ebinghaus, R., Ferrari, C., Gardfeldt, K., Goodsite, M.E., Lean, D., Poulain, A.J., Scherz, C., Skov, H., Sommar, J., and Temme, C. (2008). A synthesis of atmospheric mercury depletion event chemistry in the atmosphere and snow. Atmospheric Chemistry and Physics, 8, 1445-1482.

Silva, T. H., Garcia-Morales, V., Moura, C., Manzanares, J. A., & Silva, F. (2005). Electrochemical impedance spectroscopy of polyelectrolyte multilayer modified gold electrodes: Influence of supporting electrolyte and temperature. Langmuir, 21(16), 7461-7467.

Schlich, K., Hoppe, M., Kraas, M., Schubert, J., Chanana, M., & Hund-Rinke, K. (2018). Long-term effects of three different silver sulfide nanomaterials, silver nitrate and bulk silver sulfide on soil microorganisms and plants. Environmental Pollution, 242, 1850-1859.

Tan, S., Lee, S., Okazaki, T., Kuramitz, H., and Abd-Rahman, F. (2018). Detection of mercury(II) ions in water by polyelectrolyte-gold nanoparticles coated long period fiber grating sensor. Optics Communications, 419, 18-24.

Tang, Z., Fan, F., Wang, X., Shi, X., Deng, S., and Wang, D. (2018). Mercury in rice (*Oriza sativa L.*) and rice-paddy soils under long-term fertilizer and organic amendment. Ecotoxicology and Environmental Safety, 150, 116-122.

Thomas, R., & Swathi, R. S. (2012). Organization of Metal Nanoparticles for Surface-Enhanced Spectroscopy: A Difference in Size Matters. Journal of Physical Chemistry C, 116(41), 21982-21991.

Thomas, R., Kumar, J., George, J., Shanthil, M., Naidu, G. N., Swathi, R. S., & Thomas, K. G. (2018). Coupling of Elementary Electronic Excitations: Drawing Parallels Between Excitons and Plasmons. Journal of Physical Chemistry Letters, 9(4), 919-932.

US EPA. (1995) Water Quality Criteria Documents for the Protection of Aquatic Life in Ambient Water. United States Environmental Protection Agency, MN.

US EPA. (2007). Mercury in solids and solutions by thermal decomposition, amalgamation, and atomic absorption spectrophotometry-method 7473. United States Environmental Protection Agency, US

US EPA. (1994). Determination of mercury in water by cold vapor atomic absorption spectrometry. United States Environmental Protection Agency, US

US EPA. (1999). Compendium of methods for determination of inorganic compounds in ambient air. <u>United States Environmental Protection Agency,</u> US

Wang, T. C., Rubner, M. F., & Cohen, R. E. (2002). Polyelectrolyte multilayer nanoreactors for preparing silver nanoparticle composites: Controlling metal concentration and nanoparticle size. *Langmuir, 18*(8), 3370-3375.

Wilhelm, S.M., and Bloom, N. (2000). Review: mercury in petroleum. <u>Fuel Processing Technology</u>, 63, 1-27.

Wongsasuluk, P., Chotpantarat, S., Siriwong, W., and Robson, M. (2018). Using hair and fingernails in binary logistic regression for bio-monitoring of heavy metals/metalloid in groundwater intensively agricultural areas, Thailand. <u>Environment Research</u>, 162, 106-118.

Zhang, Y., Shoaib, A., Li, J., Ji, M., Liu, J., Xu, M., Tong, B., Zhang, J., and Wei, Q. (2016). Plasmon enhanced photoelectrochemical sensing of mercury (II) ions in human serum based on Au@Ag nanorods modified TiO2 nanosheets film. <u>Biosensor and Bioelectronics,</u> 79, 866-873.

Zhao, J. J., Bradbury, C. R., & Fermin, D. J. (2008). <u>Journal of Physical Chemistry C,</u> 112(17), 6832-6841.

APPENDICES

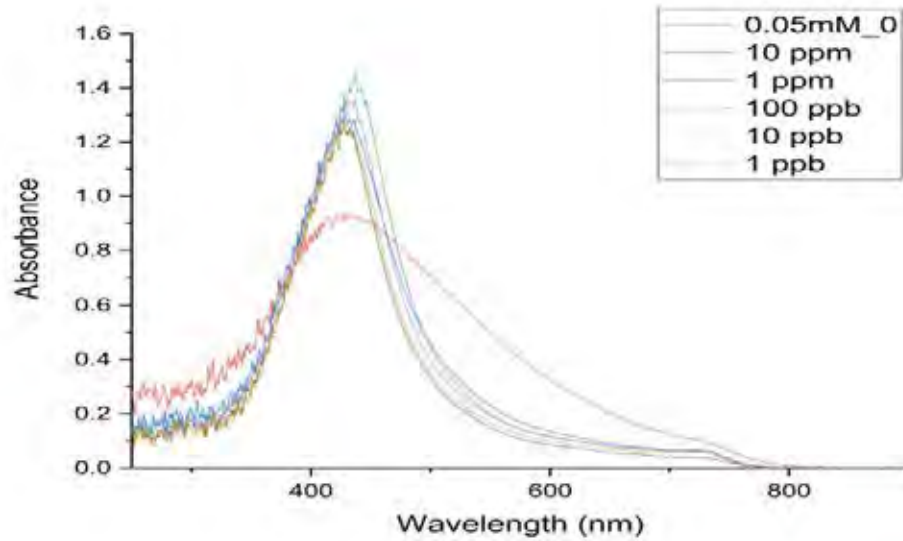**Appendix A UV-Vis Spectra of Various Capping Agent Concentration Toward Various Concentration of H₂S**

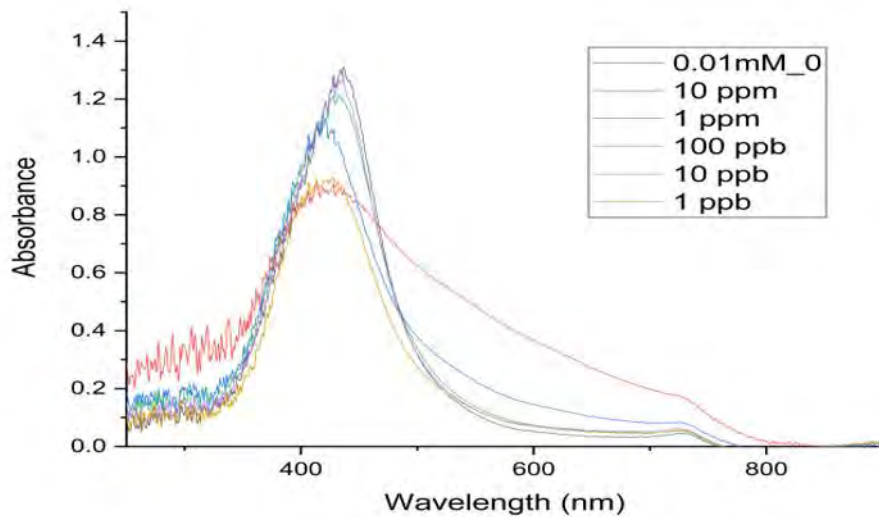**Figure A1** AgNPs with 0.05mM of CoPSS-MA to various Na2S concentrations

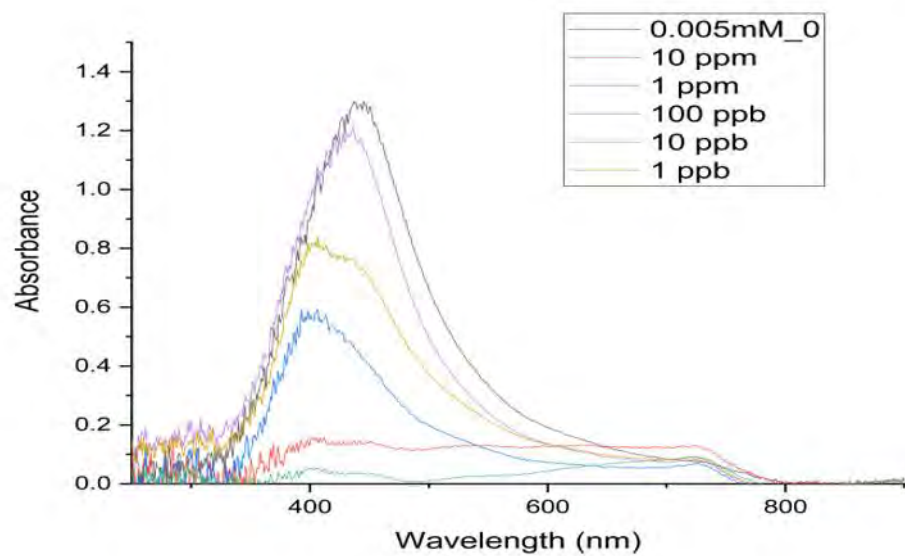**Figure A2** AgNPs with 0.001mM of CoPSS-MA to various Na2S concentrations

Figure A3 AgNPs with 0.0005mM of CoPSS-MA to various Na2S concentrations

Appendix B Ex situ and In situ AgNPs Synthesis On Glass Slide Toward Various Concentration of Na$_2$S
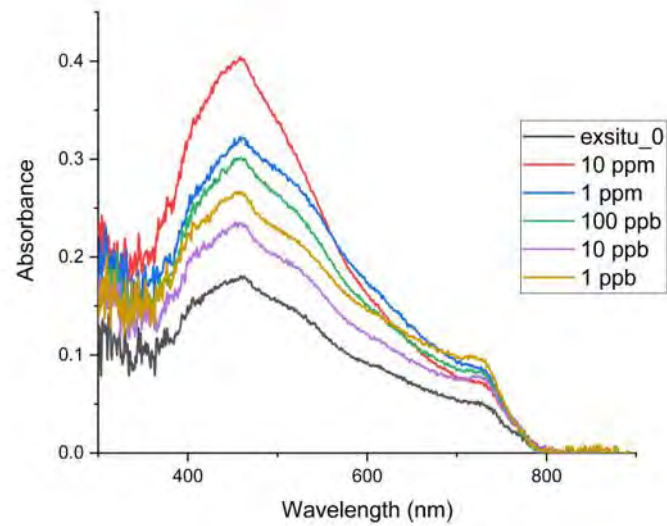

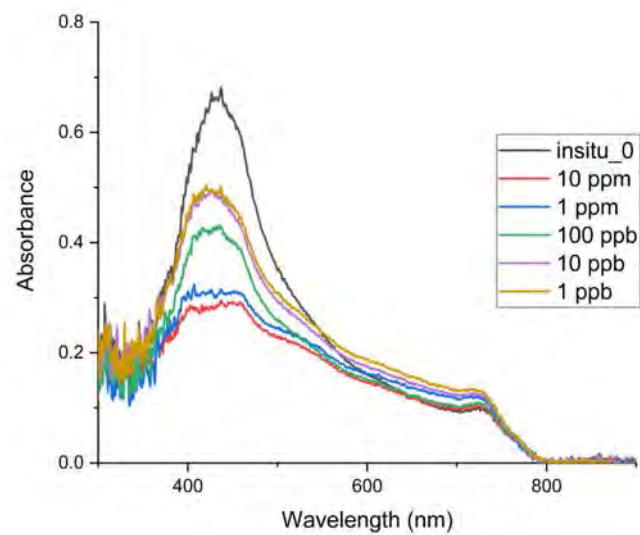**Figure B1** Ex situ AgNPs synthesis toward various concentration of Na$_2$S

Figure B2 In situ AgNPs synthesis toward various concentrations of Na$_2$S
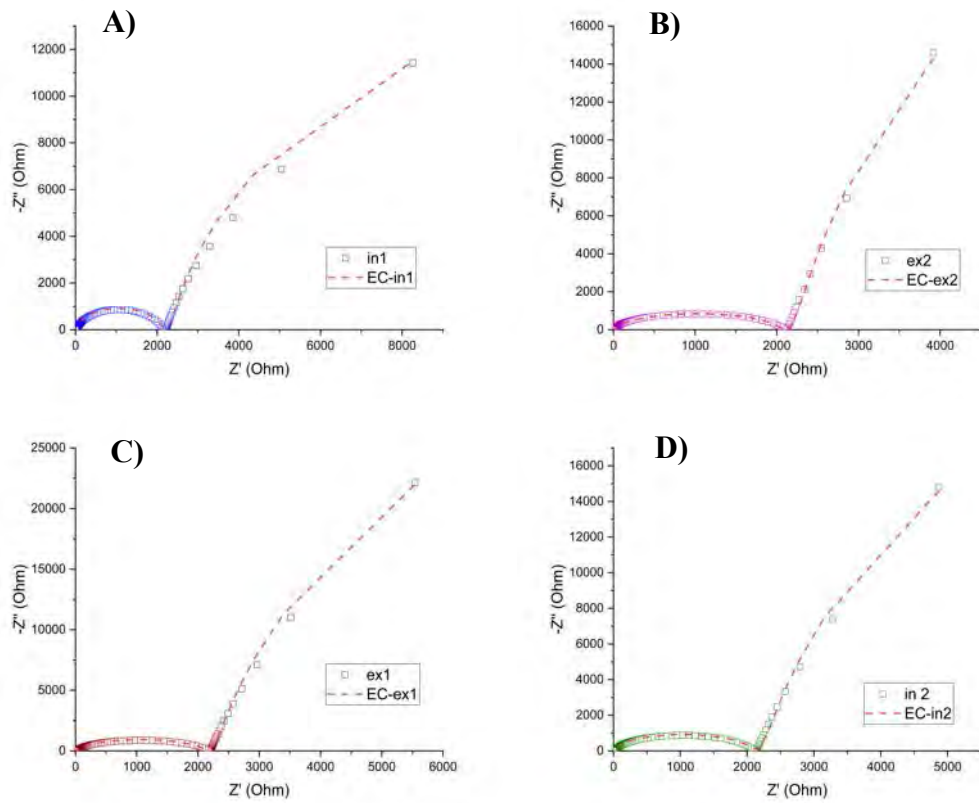
Appendix C Nyquist Plot of EC Simulation

Figure C1 Fitting equivalent circuit toward experimental result of different electrode coating and AgNPs synthesis mechanism, A) in situ in 1 electrode, B) in situ in 2 electrodes, C) ex situ on 1 electrode and D) ex situ on 2 electrodes.

CURRICULUM VITAE

Name: Mr. Muhammad Bagus Arif

Date of Birth: May 19, 1992

Nationality: Indonesian

University Education:

2012–2016 Bachelor Degree of Chemical Engineering, Faculty of Industrial Engineering, Universitas Islam Indonesia, Indonesia

Work Experience:

2017-2017   Position: Management Trainee

Company name: SLJ Global Co. Ltd., Samarinda, Indonesia

Proceedings:

1. Arif, Muhammad B. and Dubas, S. T., (2019, May 30) Silver Nano Polymer Composite Membrane for Optical Sensing of Sulfide Ion Through In situ and Ex situ Technique. Proceedings of The 10th Research Symposium on Petrochemical and Materials Technology and The 25th PPC Symposium on Petroleum, Petrochemicals and Polymers, Chulalongkorn University, Bangkok, Thailand.

Poster Presentations:

1. Arif, Muhammad B. and Dubas, S. T., (2019, May 30) Silver Nano Polymer Composite Membrane for Optical Sensing of Sulfide Ion Through In situ and Ex situ Technique. Proceedings of The 10th Research Symposium on Petrochemical and Materials Technology and The 25th PPC Symposium on Petroleum, Petrochemicals and Polymers, Chulalongkorn University, Bangkok, Thailand.